DESIGN OF A SMALL SCALE RETAINING WALL MODEL FOR INVESTIGATING THE LATERAL EARTH PRESSURES

by

Adlen Altunbaş

B.S., Civil Engineering, İstanbul University, 2009

Submitted to the Institute for Graduate Studies in
Science and Engineering in partial fulfillment of
the requirements for the degree of
Master of Science

Graduate Program in Civil Engineering

Boğaziçi University

2012

DESIGN OF A SMALL SCALE RETAINING WALL MODEL FOR INVESTIGATING THE LATERAL EARTH PRESSURES

APPROVED BY:

Assist. Prof. Özer Çinicioğlu (Thesis Supervisor)	.....
Prof. Gökhan Baykal	.....
Prof. S. Feyza Çinicioğlu	.....

DATE OF APPROVAL: 02.08.2012

ACKNOWLEDGEMENTS

I would like to express my gratitude to all the people who in one way or another contributed to the development of this research.

First and foremost, my sincere appreciation and gratitude goes to my supervisor Assist. Özer Çinicioğlu for his valuable help in instructing, sharing of knowledge, guiding and supporting me throughout the duration of this thesis.

Also, I extend my sincere thanks to the members of my Master's thesis examination committee: Prof. Gökhan Baykal and Prof. S. Feyza Çinicioğlu for their kind and supportive attitude towards me and in depth comments and advice.

My gratitude also goes to my colleague at Boğaziçi University. Special thanks to Marat Abzal for his assistance in the experiments, discussions, and sharing the ideas.

Staff of The Soil Mechanics Laboratory, Kadir Gündoğdu is thankfully appreciated for his technical help.

Above all, I would like to thank my soul mate Akın for his personal support and great patience at all times. My parents have given me their endless support throughout the thesis, as always they do.

Finally I would like to express my gratitude to The Scientific and Technological Research Council of Turkey for supporting my research through Project TUBITAK 110M595.

ABSTRACT

DESIGN OF A SMALL SCALE RETAINING WALL MODEL FOR INVESTIGATING THE LATERAL EARTH PRESSURES

The determination of geostatic stresses has a significant role on the analysis and design of various geotechnical structures, including retaining walls, piles and underground structures. Therefore correct estimation of the magnitude and distribution of the lateral earth pressures acting on geotechnical structures is of utmost importance. The goal in thesis is to design of a small scale retaining wall for investigating the parameters that influence the magnitude and distribution of lateral earth pressure for any deformation states between active and passive failure. Based on an extensive literature survey, the identified parameters of influence are arching effects, backfill friction angle, backfill density, stress level, the mode of wall movement and the frictional resistance between the wall and the backfill. To evaluate and quantify the influences of these parameters, a physical model consisting of a testing tank, a retaining wall, sand placing system, storage tank, crane and software has been developed and manufactured. LabVIEW, a system design software, is used in this model as a data acquisition system and software interface. The model is instrumented with pressure transducers and a load cell in order to measure the earth pressure at selected points on the wall and the total earth force acting on the wall. Some experiments were conducted on homogeneous normally consolidated loose uniformly graded sands in order to make sure that the physical model works properly. The results were evaluated and some interpretations were made according to experimental values.

ÖZET

YANAL TOPRAK BASINÇLARININ İNCELENMESİ İÇİN KÜÇÜK ÖLÇEKLİ İSTİNAT DUVARI MODELİ TASARIMI

İstinat duvarları, kazıklar, yeraltı yapıları gibi çeşitli geoteknik yapıların tasarımında geostatik gerilmelerin belirlenmesinin önemli rolü vardır. Bu nedenle, bu yapılara tesir eden yatay toprak basınçlarının büyüklüklerinin ve dağılımlarının doğru hesaplanması son derece önem taşımaktadır. Bu tezin amacı aktif ve pasif göçme arasında kalan deformasyon durumları için yatay toprak basınçlarının büyüklüklerini ve dağılımlarını etkileyen parametrelerinin araştırılabilmesi amacıyla küçük ölçekli bir istinat duvarı tasarlanmasıdır. Derin bir literatür araştırmasına dayanarak, bu parametreler kemerlenme etkisi, içsel sürtünme açısı, dolgu yoğunluğu, gerilme seviyesi, duvar hareketinin modu ve duvar ile dolgu arasındaki sürtünme direnci olarak saptanmıştır. Bu değişkenlerin etkilerini değerlendirmek ve sayısallaştırmak için test tankı, kum serme sistemi, kum deposu, vinç ve yazılımdan oluşan bir fiziksel bir model geliştirilmiş ve imal edilmiştir. Bu modelde data toplama işlemini yapmak ve yazılım arayüzü olarak kullanılmak amacıyla, bir sistem dizayn programı olan Labview kullanılmıştır. Model, duvar üzerinde seçilen noktalardaki toprak basıncını ve duvara etkiyen toprak kuvvetini ölçmek amacıyla basınç sensörleri ve yük sensörü ile donatılmıştır. Fiziksel modelin düzgün çalıştığından emin olmak için normal konsolide, kötü derecelenmiş, gevşek bir kum kullanılarak deneyler yapılmıştır. Elde edilen sonuçlar değerlendirilmiş ve yorumlanmıştır.

TABLE OF CONTENTS

LIST OF FIGURES

LIST OF TABLES

LIST OF SYMBOLS

c'	Effective cohesion
C_c	Coefficient of curvature
C_u	Coefficient of uniformity
D_i	Grain size corresponding to i % fines
G_s	Specific gravity of soil solids
H	Depth from the ground surface
K_a	Coefficient of active earth pressure
k_p	Coefficient of passive earth pressure
K_o	Coefficient of earth pressure at rest
$K_{o(OC)}$	Coefficient of earth pressure at rest for overconsolidated
$K_{o(NC)}$	Coefficient of earth pressure at rest for normally consolidated
m	Mass
P_a	Active forces
P_p	Passive force
S	Wall movement
p'	Mean effective stress
W_s	Weight of dry soil
W_{fs}	Weight of the flask filled with soil and water
W_{fw}	Weight of the flask filled with de-aired water only
$d\varepsilon_a$	Axial strain increment
$d\varepsilon_v$	Volumetric strain increment
ϕ	Internal friction angle
ϕ_{peak}	Peak friction angle
ϕ_r	Residual friction angle
ϕ'	Effective internal friction angle
ϕ_{cv}	Critical state friction angle
δ	Interface friction angle
γ	Unit weight

σ_1	Major principal stresses
σ_3	Minor principal stresses
σ'_a	Active effective stress
σ'_0	At rest effective stress
σ'_h	Effective horizontal stress
σ'_v	Effective vertical stress
σ'_p	Passive effective stress

LIST OF ACRONYMS/ABBREVIATIONS

$ASTM$	American society for testing and materials
MS	Moist tamping method
OCR	Overconsilidation ratio
WS	Water sedimentation method

1. INTRODUCTION

The aim of thesis is to design a small scale retaining wall model for calculating the lateral earth pressure coefficients of cohesionless soils. The determination of lateral earth pressure coefficients has a significant role on the design of many geotechnical structures. Hence, correct estimation of the magnitude and distribution of the lateral earth pressures acting on geotechnical structures is of utmost importance.

For this purpose, a physical model is designed and manufactured in soil mechanics laboratory to investigate the lateral earth pressures acting on geotechnical structures retaining cohesionless backfills. This model consists of a testing tank, a retaining wall model, a sand placing system, storage tank, crane and and a software. The sides of the testing tank are plexiglass allowing the observation of deformations during testing, thus visual analyses of the tests can be conducted using particle image velocimetry (PIV) method. As a results of this, the failure surface geometry can be observed and its impacts can be investigated. In addition to fact that the relationships between K_o - K_a and K_o - K_p can be defined as functions of the density and overconsolidation ratio by means of the data obtained using the new model.

After finishing the designing of the model, several experiments were conducted to confirm the accuracy of measurements, to identify the repeatability of the tests, and to verify the extent of our control over the prepared models. The results were compared with the theories and with the previous research in the field. As a result of this verification experiments, it could be decided that the model works accurately. Test results also evaluated and compared with previous the literature.

2. LITERATURE REVIEW

2.1. Earth Pressure at Rest

Based on an extensive literature survey, many reports suggest different approaches for the calculation of lateral earth pressure coefficients for at rest states, especially in the case of normally consolidated soils. It is possible to argue that there is a consensus among researchers so that the lateral earth pressure coefficient for at rest states is directly a function of the internal friction angle, ϕ'. Internal friction angle of the soil is considered as the only parameter controlling the values of the earth pressure coefficient for normally consolidated soils (Jàky, 1944; Terzaghi, 1920). However, there are also several empirical formulas proposed for predicting the earth pressure coefficient at rest for overconsolidated cohesionless soils (Wroth, 1973; Meyerhof, 1976; Mayne and Kulhawy, 1982; Duncan and Seed 1986; Hanna and Ghaly, 1992; Mesri and Hayat, 1993). Nevertheless, wide discrepancies can be found between the results used by these formulas. Some researchers have investigated the underlying reasons of these discrepancies.

Jàky (1944) studied the stress field in a wedge prism of normally consolidated loose granular materials as shown in Figure 2.1. He asserted that the stress on the central vertical plane of the wedge prism was the pressure at rest.

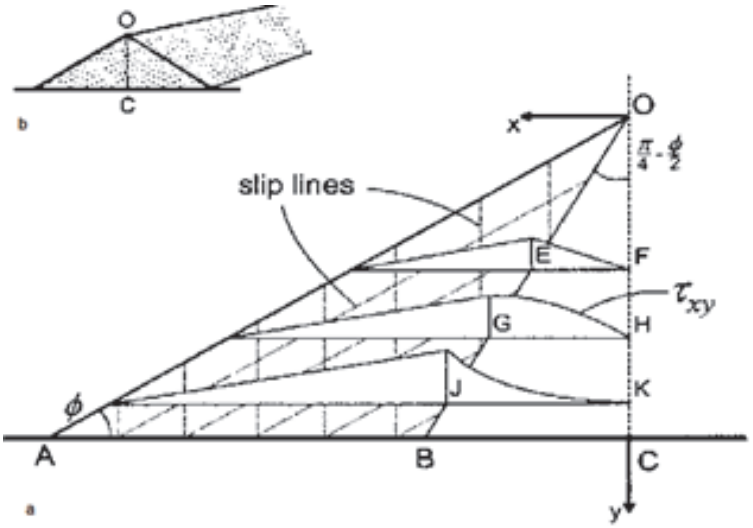

Figure 2.1. Wedge-shaped sand prism: (a) schematic of a long mound (plane strain analysis); and (b) cross section of a symmetric half (Michalowski, 2005).

Jàky (1944) suggested that the lateral earth pressure coeffient at rest, K_o, for normally consolidated soils could be calculated with using Jàky's equation:

$$K_o = \sigma_h/\sigma_v = (1 + \frac{2}{3}sin\phi')\frac{1 - sin\phi'}{1 + sin\phi'} \approx 0.95 - sin\phi' \tag{2.1}$$

or approximately

$$K_o = (1 - sin\phi') \tag{2.2}$$

where ϕ' is effective friction angle. It is necessary to emphasize the fact that Jàky's equation was obtained for normally consolidated soils. It can be said that the effect of overconcolidation not considered in Jàky equation.

Feda (1983) based his investigations on the experimental verification of Jàky's formula. According to Feda's investigation, Jàky's formula has some limitations. First, some experimental results deviate considerably and cannot be expressed by this formula (Holtz and Kovacs, 1981). Second, although K_o is a deformation parameter, Jàky's formula claims the dependence of K_o on the strength parameter. Feda (1983) used dry

medium Zbraslav sand (grain was tested at different diameter $\leq$ 2 mm, 90% of grain size in the 0.1-1 mm range) in his investigation. The standard triaxial apparatus with sample diameter about 3.8 cm and height to diameter ratio of about two was used in his investigation. Based on the results, he asserted that Jaky's formula cannot be generally accepted. His experiments affirmed Jaky's formula for dense sand only. Feda (1983) claimed that for further increase of overconsolidated ratio (OCR) the value of $K_{o(OC)}$ decreases as shown in Figure 2.2. In other words, maximum $K_{o(OC)}$ does not correspond to the maximum OCR (Feda, 1983).

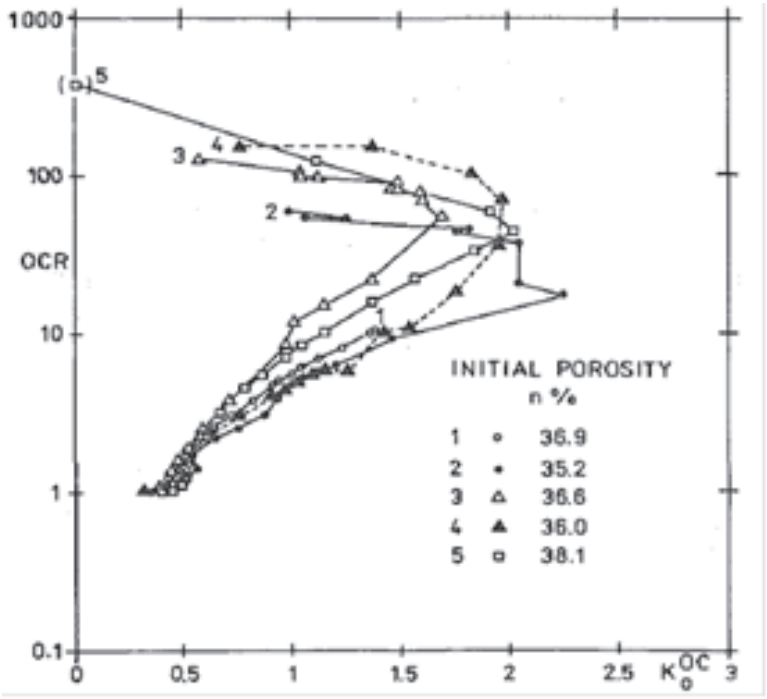

Figure 2.2. Relationship between overconsolldation ratio (OCR) and coefficient of earth pressure at rest $K_{o(OC)}$ during loading (Feda, 1983).

Mayne and Kulhawy (1982) investigated K_o-OCR relationships in soil. According to an extensive review of laboratory data of over 170 soils, Mayne and Kulhawy (1982) obtained that Jàky's equation could be valid for cohesive soils and moderately valid for cohesionless soils. The values of K_o, void ratio and friction angle are all available for 27 materials in Mayne and Kulhawy's database. They divided the data in two groups, A and B as shown in Figure 2.3, respectively. The K_o-values of soils in group A can be estimated by Jàky's equation within $\pm$0.05. In group B, a statistical analysis

shows that 72% of experimental K_o-values in this group vary within ±0.1 of the Jàky's relationship in the form of either Equation 2.1 or Equation 2.2. Mayne and Kulhawy (1982) suggested an improved fitting which obtained with 72% data located within ±0.03 of this relation when the constant C is appropriately selected. Mayne and Kulhawy (1982) claimed that only the effective stress friction angle and prior stress history are needed to estimate the approximate values of K_o

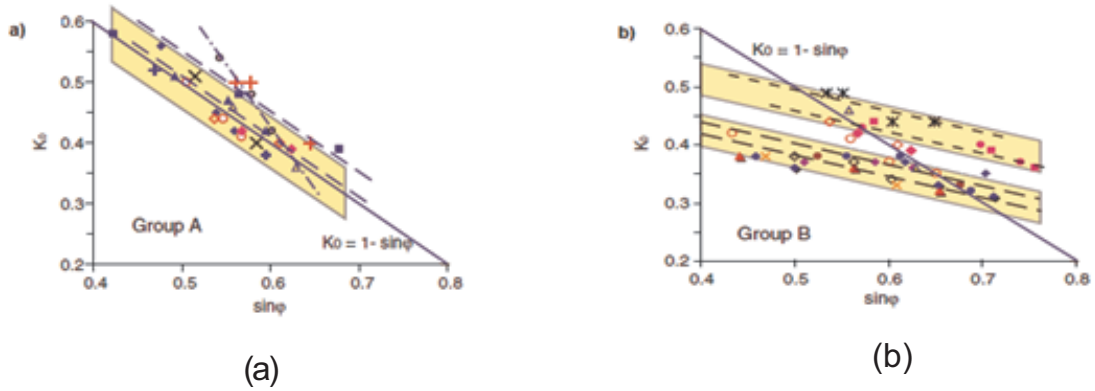

Figure 2.3. Variation of K_o -values of cohesionless soils (Peijun Guo, 2010).

Okochi and Tatsuoka (1984) investigated the factors affecting K_o -values of sand. They used a double cell K_o triaxial apparatus, in which the zero lateral strain condition was obtained by maintaining the constant volume of de-aired water in the annular space between the inner cell and the outer cell while the resulting cell pressure was measured using a differential pressure transducer. They conducted this test for two types of samples, namely wet-tamped specimens and airpluviated samples. They noted that the K_o of wet-tamped specimens calculated from K_o=σ'_h/σ'_v could be described by Jàky's equation. However, the K_o of airpulvinated samples, which were normally consolidated, were 10 to 15% higher than that of wet-tamped specimens with the same void ratio. It could be attributed to the different internal structures and grain packing related to different sample preparation methods.

Chu and Gan (2004) investigated the K_o values of loose sand by performing controlled strain-path triaxial compression tests on saturated specimens. They controlled the ratio between the volumetric strain increment and the axial strain increment to

obtain the K_o condition; i.e., $d\varepsilon_v/d\varepsilon_a = 1$, which implied that the lateral strain increment $d\varepsilon_r = 0$. They terminated their test when the mean effective stress, p' , reached 300kPa. They suggested that K_o values were significantly affected by void ratio. In addition to that his results are lower than that predicted by Jàky's theory. They also observed that samples prepared by wet-tamping had higher K_o values than those prepared by water pluviation. Figure 2.4 summarizes the experimental data reported by Chu and Gan (2004) as well as Okochi and Tatsuoka (1984). They concluded that K_o may not be uniquely determined by friction angle without taking into account the effect of density and fabric of the specimens. In addition these parameters, OCR, stress level, homogeneity may affect K_o values. It may be said that stress level may influence void ratio, density, soil structure, homogeneity, grain packing, etc. For this reason, stress level should also be considered.

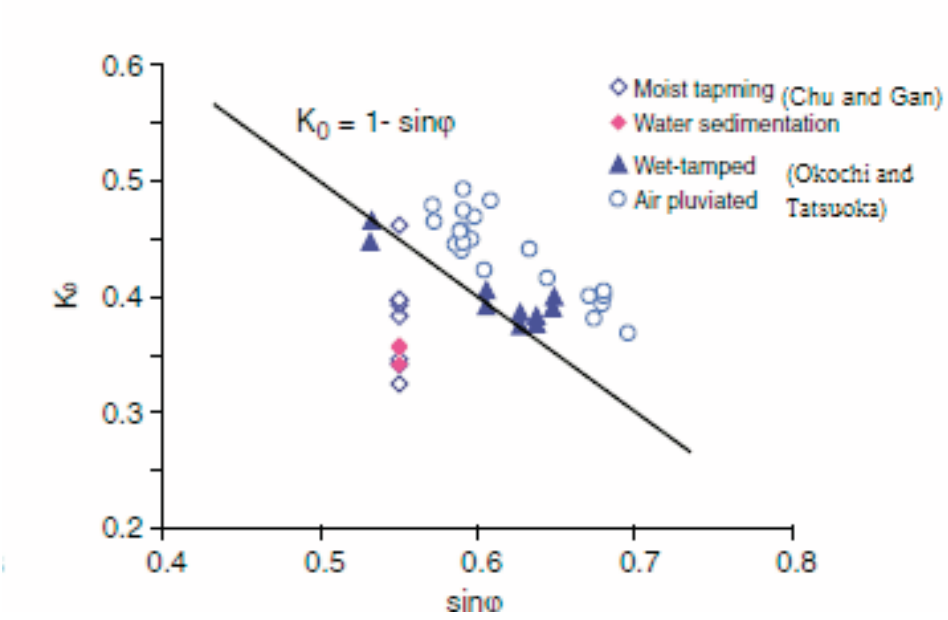

Figure 2.4. Variation of K_o -values of cohesionless soils (Peijun Guo, 2010).

Michalowski (2005) reveals that the problem of wedge-shaped sand prism in Figure 2.1 is not related to the stress path typical of a one-dimensional strain process associated with the K_o state and Jàky's solution may result in a rather peculiar stress distribution at the base of the prism. He illustrated that Jàky's solution is not a precise theoretical prediction of the earth pressure at rest. He claimed that the coefficient of at rest depends on the history of deposition of the granular material.

Wanatowski and Chu (2007) investigated K_o of sand measured by a plane -strain apparatus. They compared their results with the K_o measured by triaxial K_o consolidation test. They used two different types of sample preparation methods, namely water sedimentation method (WS) and moist tamping method (MT). They observed that the K_o values determined by plane strain tests are in good agreement with the values determined by triaxial tests. It can be seen from Figure 2.5, they observed that the K_o values obtained from the tests on the water sedimentation specimens show little dependence on the initial void ratio, thus do not agree with K_o values calculated from Jàky's equation using the peak friction angles obtained from either triaxial test or plane strain test. The K_o values obtained from the tests on moist tamping specimens form a linear relationship with void ratio. However, this relationship also does not agree with Jàky's theory. Chu and Gan (2004) reached the same conclusion when investigating effect of void ratio on K_o of loose sand. In other words, Chu and Gan (2004) observed that specimens using the moist tamping method, the K_o values and strain-stress behavior are considerably depend on void ratio. However, the effect of void ratio on K_o is less significant for specimens prepared using the water sedimentation. In addition to these, the K_o values obtained from the experiments are lower than that predicted by Jàky's equation. Wanatowski and Chu (2007) concluded that the difference in the K_o values measured for the WS and MS specimens appears to be related to the differences in the soil fabrics and structures, resulting from different specimen preparation methods. The structure should be defined by additional parameters, such as sample fabric, homogeneity, grain packing etc.

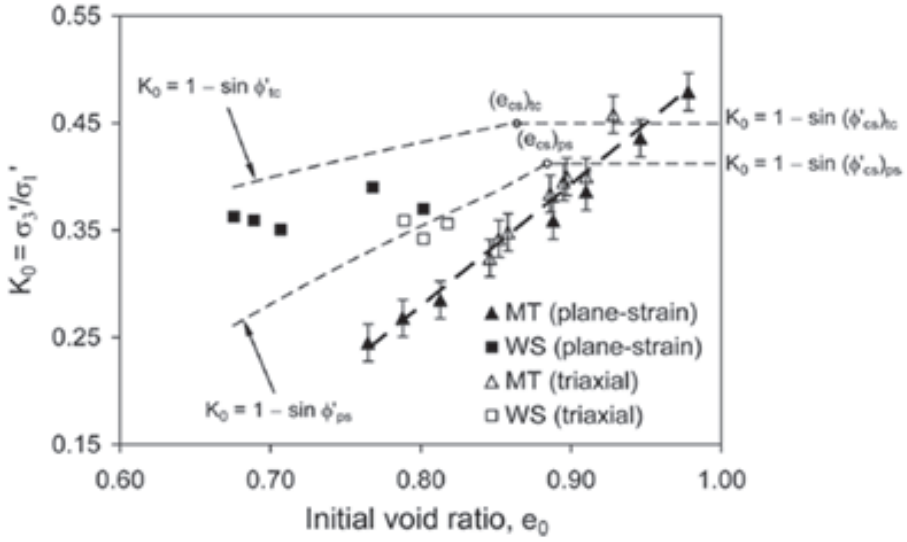

Figure 2.5. Summary of K_o consolidation test (adapted from Wanatowski and Chu 2007).

Hanna and Al-Romhein (2008) conducted an experimental investigation. Their objective was to report the results of the experiments for understanding the at-rest earth pressures acting on retaining walls. They evaluated the empirical formulas proposed by Wroth (1973), Meyerhof (1976), and Mayne and Kulhawy (1982) which are given in Equations 2.3 to Equations 2.5, respectively. These are equations that are commonly used in practice to predict K_o.

$$K_{o(OC)} = K_{o(NC)}OCR - [\frac{\mu}{1-\mu}](OCR - 1) \tag{2.3}$$

where $\mu = 0.1 - 0.3$ for loose sands; $\mu = 0.3 - 0.4$ for dense sands; and μ is Poisson's ratio.$K_{o(NC)}$ is the coefficient of earth pressure at rest for normally consolidated sand; and $K_{o(OC)}$ is the coefficient of earth pressure at rest for overconsolidated sand.

$$K_{o(OC)} = (1 - sin\phi')\sqrt{OCR} \tag{2.4}$$

$$K_{o(OC)} = (1 - sin\phi')OCR^{sin\phi'} \tag{2.5}$$

Hanna and Al-Romhein (2008) used overconsolidated homogeneous dense, medium, and loose sands for the experimental investigation. They designed a testing tank, a retaining wall, and a sand placement system in order to investigate the at-rest earth pressure acting on the wall. They used well-graded, dry silica sand for the experiment. The maximum and the minimum void ratios of the sand were 0.52 and 0.33, respectively. The unit weight of the sand varied between 17.41 and 19.95 kN/m^3. They used direct shear box test to determine the angle of shearing resistance of the sand and the angle of friction between the sandpaper and the sand. Based on the experimental results, they suggested that the coefficient of earth pressure at rest is a function of the angle of shearing resistance and the overconsolidation ratio (OCR) of the sand. Additionally, they explained OCR as a function of the degree of the interlocking of the soil particles, stress history and sand-placing techniques used in the laboratories. They concluded that the coefficient of earth pressure at rest increases significantly with an increase of the OCR. However, Feda (1983) claimed that for further increase of OCR the value of $K_{o(OC)}$ decreases. Hanna and Al-Romhein (2008) asserted that the theoretical values calculated by the conventional methods were in good agreement with the experimental results for OCR values of up to 3. Hanna and Al-Romhein (2008) also claimed that the angle of friction between the wall and the sand did not have any effect on the measured coefficient of earth pressure at rest. The reason for this inference is that the settlement of the retained soil in not large enough to fully induce friction between the walls and the soil.

Guo (2009) conducted an investigation about the effects of density and compressibility on K_o of cohesionless soils. The objective of his investigation is to re-examine the variation of K_o of granular soils with material properties in addition to the friction angle to obtain an improved prediction for K_o Guo (2009) focused on the correlation of K_o with compressibility and density by considering the influence of stress level. Guo (2009) used two types of granular soils to obtain their K_o values at different void ratios. These are Ottawa sand C109 (Sand O) and a sand derived from crushed limestone (Sand L), with the basic physical properties listed in Table 2.1.

Guo (2009) used oedometer tests to obtain the compressibility properties of the

Table 2.1. Physical properties of testing materials.

Material	Particle Shape	e_{max}	e_{min}	D_{10} (mm)	D_{50} (mm)	C_u	ϕ_{cv} (^{0})
Sand L	Angular	1.2	0.52	0.95	1.64	1.95	37
Sand O	Rounded	0.81	0.5	0.22	0.38	1.80	32

materials. He also performed series of traditional triaxial compression tests in order to obtain the internal friction angle and the dilatancy of the material with different densities under various confinements. He measured K_o values by using controlled strain-path triaxial tests when the strain increment ratio $d\varepsilon_v/d\varepsilon_a$ is unity as described by Chu and Gan (2004) and Chu and Lo (1991). The variation of peak friction angles in triaxial compression with the void ratio and the effective confining pressure is presented in Figure 2.6. It can be seen from Figure 2.6 that increased confining pressure and void ratio both reduces the peak friction angle and dilation. In the range of $\sigma_h = 50 - 200$ kPa, however, the influence of stress level is not as significant as that of void ratio as can be seen in Figure 2.6.

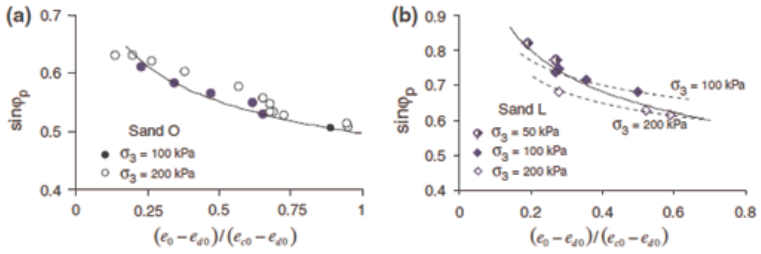

Figure 2.6. Dependency of peak friction angle on (e_0- e_{d0})/ (e_{c0}- e_{d0}) (Guo, 2009).

Guo (2009) concluded that the coefficient of earth pressure at rest K_o of granular materials is not a unique function of neither the critical friction angle, ϕ_{cv}, the peak friction angle, ϕ_p . He significantly illustrated that the effect of density and stress level on K_o should be considered.

As per the above review, the parameters that influence the coefficient earth pressure at rest are OCR, friction angle, different sample preparation method attributed to the different internal structure, density, fabric of the specimen, initial void ratio, stress

level, homogeneity, grain packing, material properties, mean grain size diameter and grain shape.

2.2. Passive Earth Pressure

As it is well known, passive earth pressures play a significant role in soil-structure interaction. In order to calculate correct passive pressure values, some theories were suggested. Two of them are commonly used in geotechnical engineering, namely Coulomb Theory and the Rankine Theory. Coulomb theory tackles the pressure problems in terms of force, and Rankine theory tackles the problems in terms of stress. The logarithmic spiral earth pressure theory developed by Terzaghi (1941) is less widely used than the Coulomb and Rankine theories owing to its complexity.

Many researchers had developed passive pressure coefficients, e.g., Coulomb (1776), Rankine (1857), Caquot and Kerisel (1948), Brinch-Hansen (1953), Janbu (1957), Sokolovski (1960), Terzaghi and Peck (1967). However, it can be said that these passive pressure coefficients are based on the frictional resistance alone.

Coulomb is considered to be the first scientist to develop a theory to predict the passive earth pressure coefficient. He investigated earth pressure coefficients and proposed empirical formula Equation 2.6. In this formula, he assumed that the failure surface in the backfill is planar, as shown in Figure 2.7. In addition to this assumption, Coulomb (1776) assumed in his investigation that:

(i) Soil is isotropic and homogeneous. It has both internal friction and cohesion.
(ii) Failure is a plane strain problem.
(iii) The failure wedge is a rigid body undergoing translation.
(iv) The friction resistance is distributed uniformly along the rupture surface and soil-to-soil friction coefficient is $f = tan\phi$.
(v) Friction forces are developed between the wall and the soil.
(vi) The extreme values of force determined by Coulomb theory are expressed as:

$$P_{a(P)} = \frac{1}{2} K_{a(P)} \gamma H^2 \tag{2.6}$$

In which, P_a, P_p and K_a, K_p are active and passive forces and earth pressure coefficients, respectively.

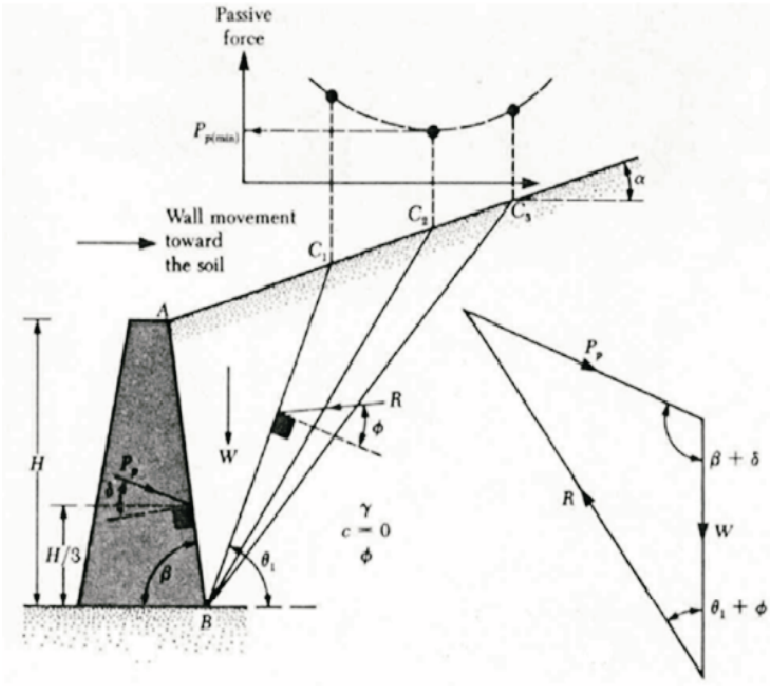

Figure 2.7. Passive wedge calculated with Coulomb's theory.

Rankine (1857) considered soil in a state of plastic equilibrium and used essentially the same assumptions as Coulomb. In Rankin's theory, the different thing is that he assumed no wall friction or soil cohesion. According to Rankine theory, the active effective stress is expressed as:

$$\sigma'_a = \sigma'_o tan^2(45^o - \frac{\phi'}{2}) - 2c' tan(45^o - \frac{\phi'}{2}) \tag{2.7}$$

And the passive effective stress as:

$$\sigma'_p = \sigma'_o tan^2(45^o + \frac{\phi'}{2}) + 2c' tan(45^0 + \frac{\phi'}{2}) \tag{2.8}$$

in which, ϕ' is effective friction angle and c' is effective cohesion.

The first known advanced measurements of horizontal passive earth pressure appeared to be those of Terzaghi (1920). He indicated that, the real surface of the sliding in the backfill consists of a curved lower part and a straight upper part owing to the influence of wall friction. As a wall pushes toward the retained backfill, the straight portion of the sliding surface rises at an angle of 45^o - (ϕ) /2 with the horizontal, as shown in Figure 2.8. The area ADF is in the passive Rankine state and the curved part of the surface of sliding BCD was assumed to be a logarithmic spiral.

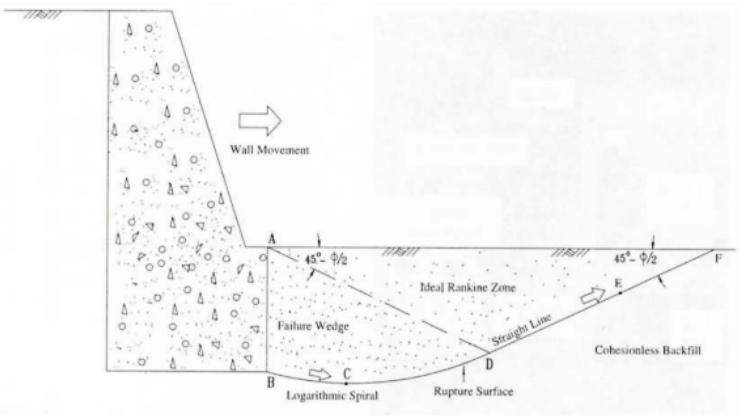

Figure 2.8. Passive wedge calculated with Terzaghi's log-spiral method (Fang and Lee, 2006).

Terzaghi (1920) used a 2 inch high wall to measure passive earth pressure coefficients. Passive earth pressure coefficients were observed to be greater than 10 for dense sand after smaller wall movements, and well in the excess of the value of two for loose sand at a wall movement equal to 15% of its height. Based on experiments, Terzaghi had obtained that the translational movement of a retaining wall influences the horizontal passive earth pressure against the wall. Terzaghi (1920) illustrated that Coulomb ignored that the sand consists of grains, and he dealt with the sand as if it was homogeneous mass with certain mechanical properties.

Terzaghi (1934) conducted several large-scale retaining wall tests with dry sand backfill. He concluded that the unit weight of the backfill affects the lateral pressure

on the retaining walls. In addition to this, the amount of wall movement considerably influences the lateral pressure on the retaining walls. He also claimed that the soil friction angle and the wall friction vary during wall movement. As a result of this, the resultant pressures acts at a point higher than the lower third point proposed by Coulomb.

Rowe and Peaker (1965) measured the passive earth pressure on a vertical wall moved by translation against a horizontal fill. Their test apparatus consist of a bin 4.3 m $\times$ 2.7 m in a new 60-ton sand flume. The wall was 1.8 m wide and 0.45 m high and consisted of three separate sections each 0.6 m wide. The central section housed three columns of six earth pressure cells. They used this equipment to control the wall direction and the consequent rate of mobilization of wall friction. Based on the tests' results, Rowe and Peaker (1965) observed that the distribution of pressure on the translating wall was essentially linear in all the tests at each part of deformation up to failure.

Rowe and Peaker (1965) also found that the angle of wall friction, δ, changed in relation to the rate of wall displacement. They showed that the rate of displacement depends on the instantaneous direction of the wall movement from the horizontal and the volume change rate of the sand behind the wall at each stage of the tests as shown in Figure 2.9 and Figure 2.10.

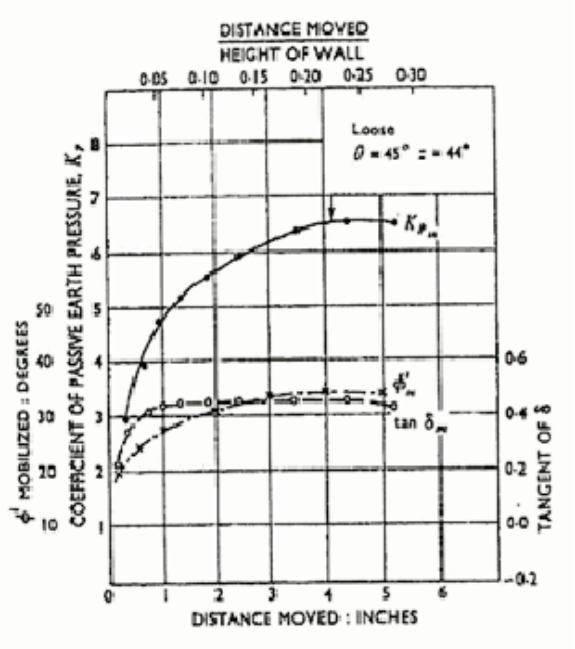

Figure 2.9. K_p and wall friction for loose sand (Rowe and Peaker, 1965).

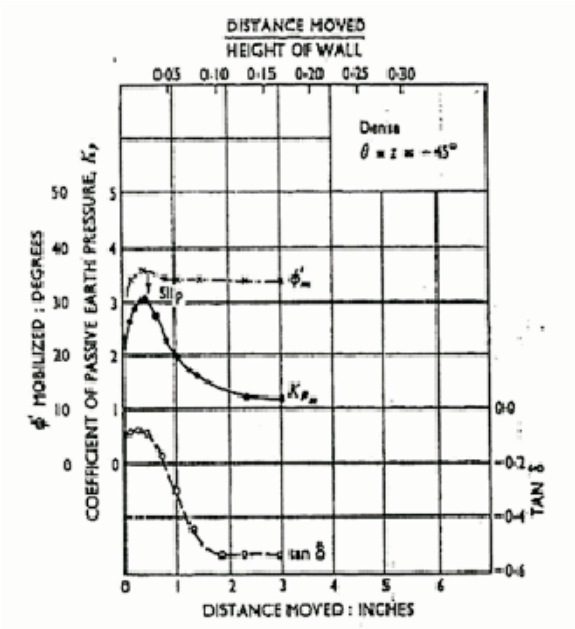

Figure 2.10. K_p and wall friction for dense sand (Rowe and Peaker, 1965).

Rowe and Peaker (1965) claimed that the passive earth pressure coefficient K_p, the soil friction angle, ϕ and the wall friction angle, δ, increased initially with the increase of the wall's translational movements and kept constant after they reached peak values as shown in Figure 2.11.

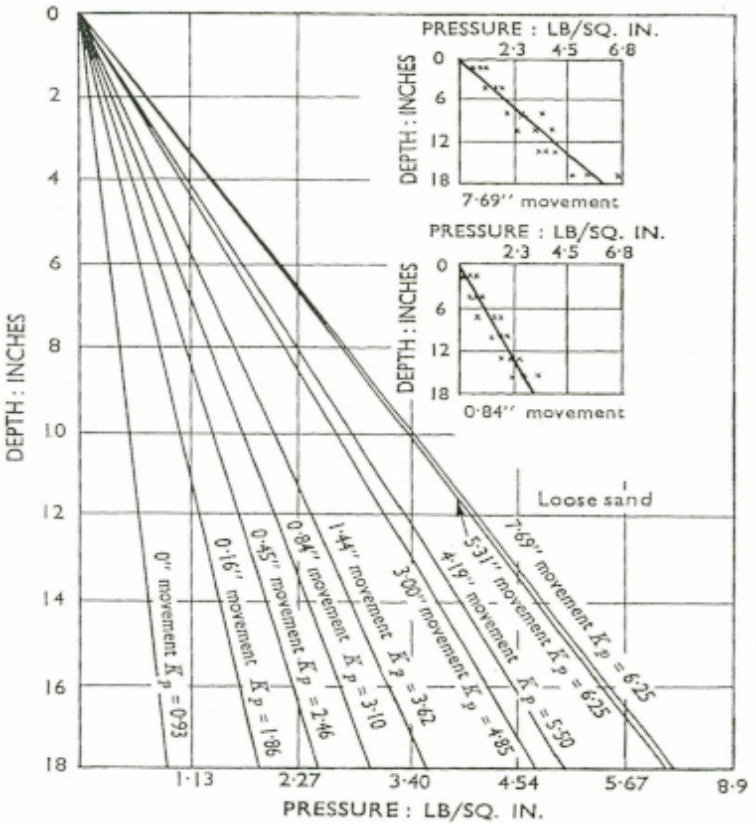

Figure 2.11. Typical pressure distribution (Rowe and Peaker, 1965).

Rowe and Peaker (1965) claimed that neglecting the effect of the displacement on the soil's friction angle, ϕ, and wall friction, δ, would yield to errors in the use of all the theories. Their tests also showed that for loose sand, the observations are in good agreement with that predicted by theories only after large wall displacements. For dense sand, progressive failure of elements in the mass lead to average maximum Coulomb values of ϕ' that are smaller than those predicted by the plane strain compression tests.

D'Appolonia (1967) reported that if the backfill was loose, the passive earth pressure obtained experimentally compared well with those obtained from Coulomb theory as observed by c if the backfill was dense, the Coulomb solution was approximately 100% higher than the experimental results.

Many researchers such as Narain and Nandakkumaran (1969), Fang *et al.* (1994) had noticed that in addition to wall translation, wall rotation also induces passive earth

pressure.

Narain and Nandakkumaran (1969) conducted series of tests with both loose and dense sand in order to investigate the passive earth pressure acting on a rigid retaining wall under three different wall movements in Figure 2.12, namely translation and rotations about its top or toe.

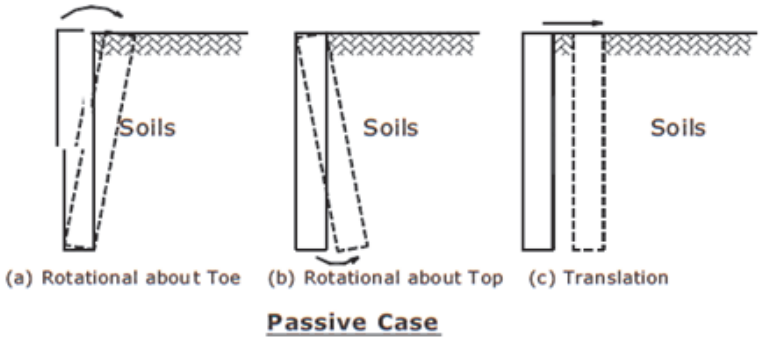

Figure 2.12. Rotational and translational retaining wall movement for passive case (Sherif *et al.*, 1984).

From the test results shown in Figure 2.13 and Figure 2.14, Narain and Nandakkumaran obtained that:

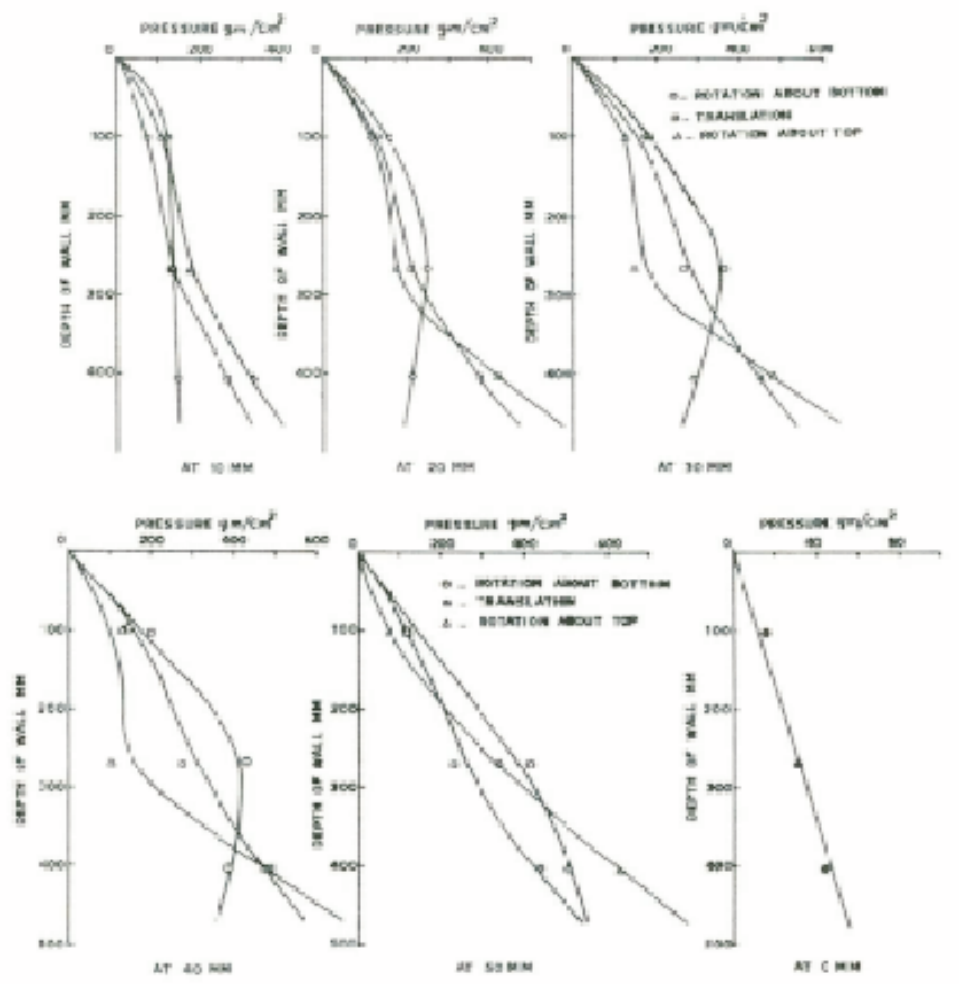

Figure 2.13. Pressure distribution on the wall at different wall movements (loose sand passive case) (Narain and Nandakkumaran, 1969).

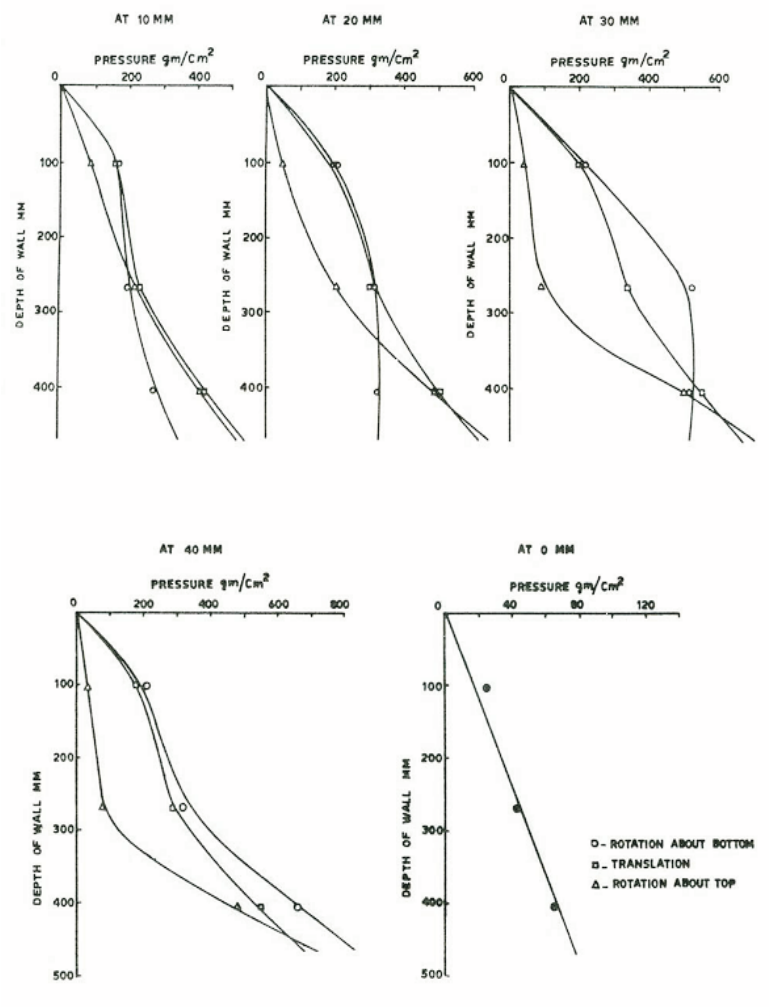

Figure 2.14. Pressure distribution on the wall at different wall movements (dense sand passive case) (Narain and Nandakkumaran, 1969).

Narain and Nandakkumaran (1969) claimed that pressure distribution along the wall height was linear for the translational wall movement. They explained that a different wall movement, the pressures at different depths increased with the increase in wall displacements and the maximum pressure at all depths were reached simultaneously. Passive earth pressure coefficient increased with wall movements until a maximum value was reached. Similar results were obtained by Rowe and Peaker (1965), and Fang *et al.* (2001). Fang *et al.* (1994, 2001) indicated that Rankine theory underestimated the passive thrust, whereas Coulomb theory overestimated the passive pressure. However, experimental values were in good agreement with Terzaghi's prediction based on the general wedge theory as shown in Figure 2.15. According to Narain and Nandakku-

maran (1969), the maximum passive earth pressure obtained at a wall displacement accounting to 8.6% and 6.4% of the wall's height, when translating in loose and dense sands respectively. In addition to these observations, Fang *et al.* (1994, 2001) claimed that as the wall movement exceeded 12% of the wall height, the passive earth pressure would reach the maximum constant value, regardless of the initial density of the backfill as shown in Figure 2.16.

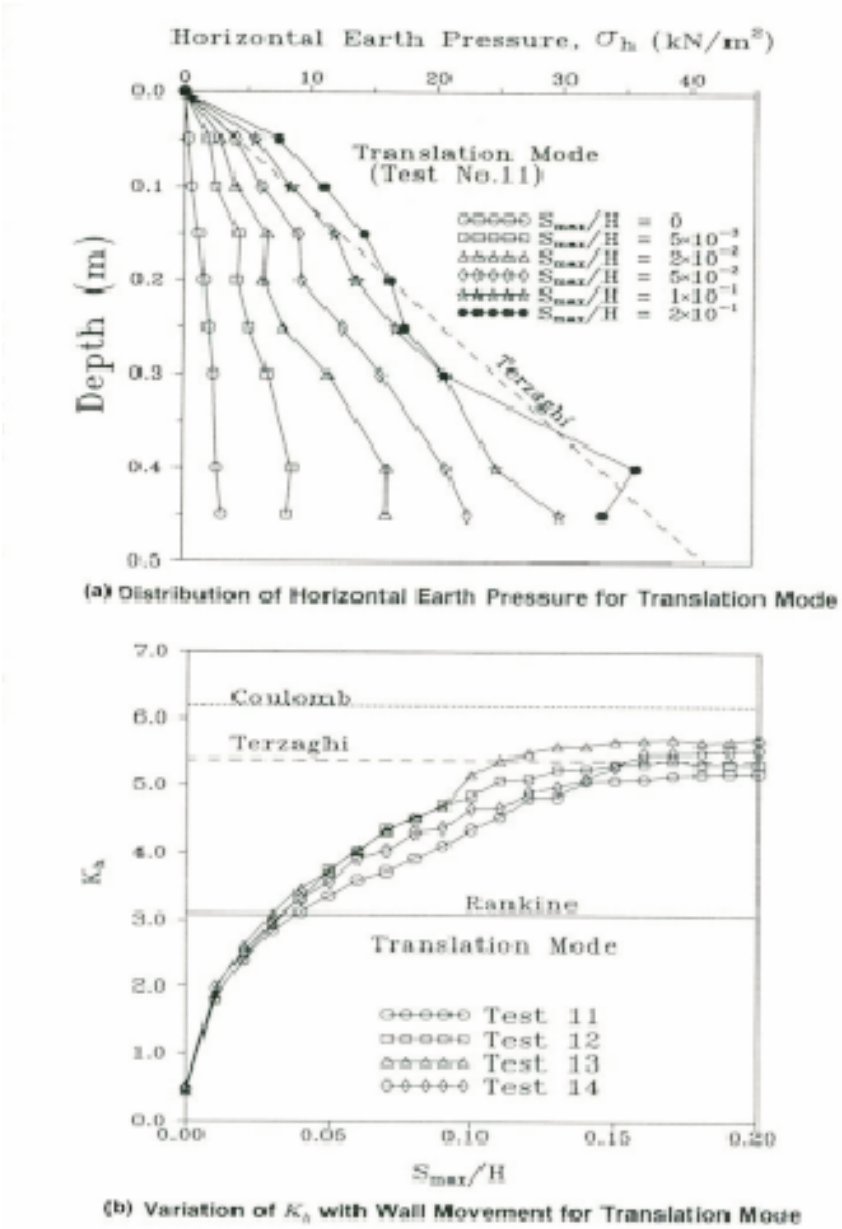

Figure 2.15. Distribution of horizontal earth pressure for translation mode, Variation of K_p with wall movement for translation mode (Fang *et al.*, 1994).

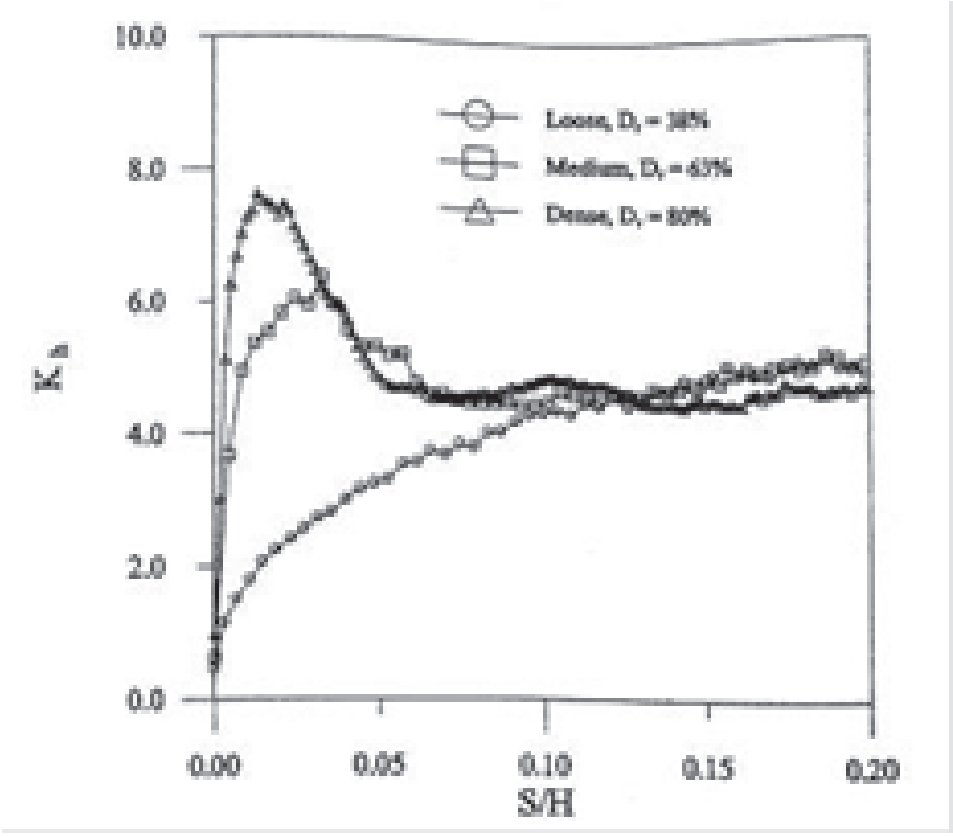

Figure 2.16. Variation of K_p with wall movement for loose, medium dense, and dens backfill (Fang *et al.*, 2001).

Narain and Nandakkumaran (1969) also investigated on passive earth pressure distrubution when wall rotation about its top. The displacement of the wall required to cause the maximum coefficient of passive earth pressure equaled to 6.6% and 3.3% of the wall height for loose and dense sand, respectively. According to Fang *et al.* (1994) observations as shown in Figure 2.17 and Figure 2.18, pressure measured near the lower edge of the wall increased with wall rotation before reaching an ultimate value. The pressure near the top did not change considerably. There were some discrepancies between the displacement models proposed by Narain and Nandakkumaran (1969) and those proposed by Fang *et al.* (1994).

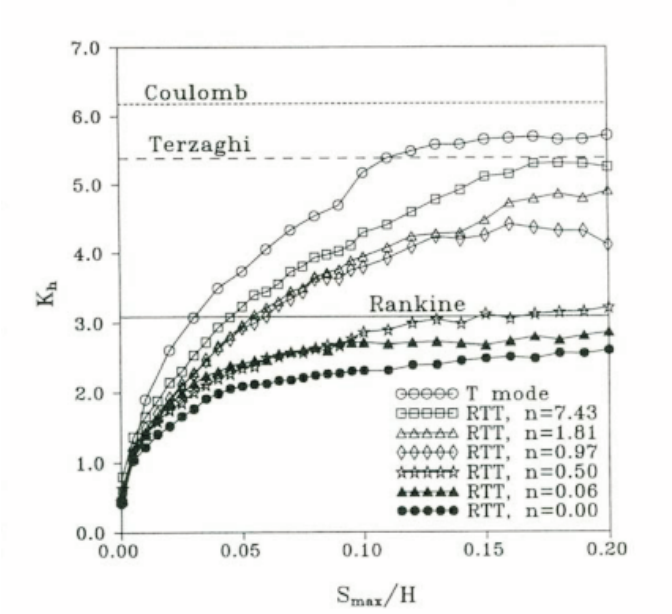

Figure 2.17. Variation of K_p with wall movement for RTT (rotation about a point above the top) mode (Fang et al. 1994).

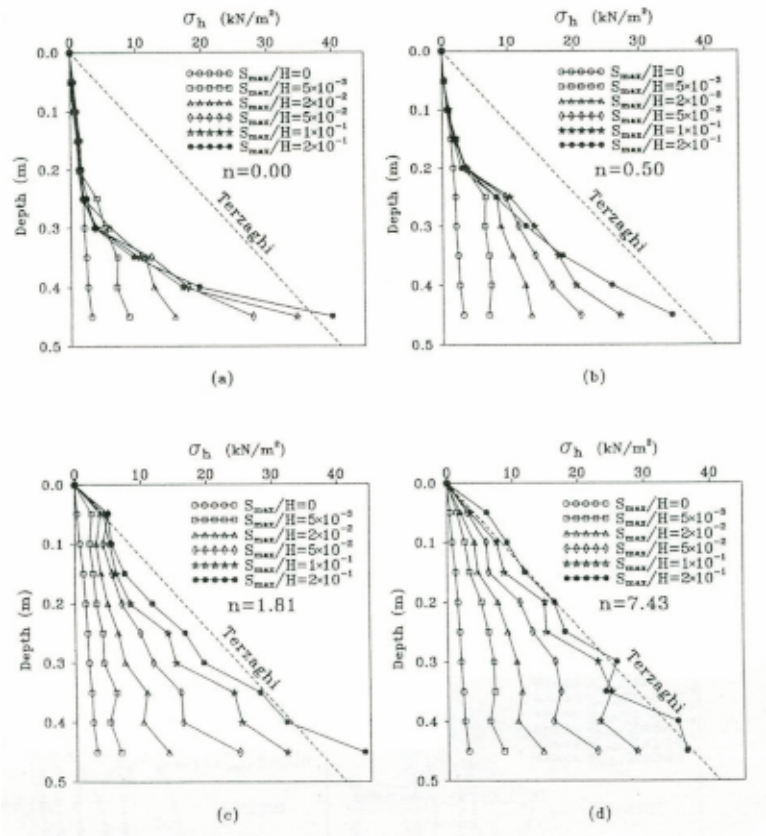

Figure 2.18. Distribution of horizontal earth pressure for RTT (rotation about a point above the top) mode (Fang et al. 1994).

In addition to these results, Narain and Nandakkumaran (1969) tried to find the effect of wall rotation about its toe. They obtained that the maximum values of pressures were not reached simultaneously at all points. The pressure distribution on the wall was far from being triangular and approximated a parabola. Similar observations were reported by Fang *et al.* (1994) as shown in Figure 2.19 and Figure 2.20.

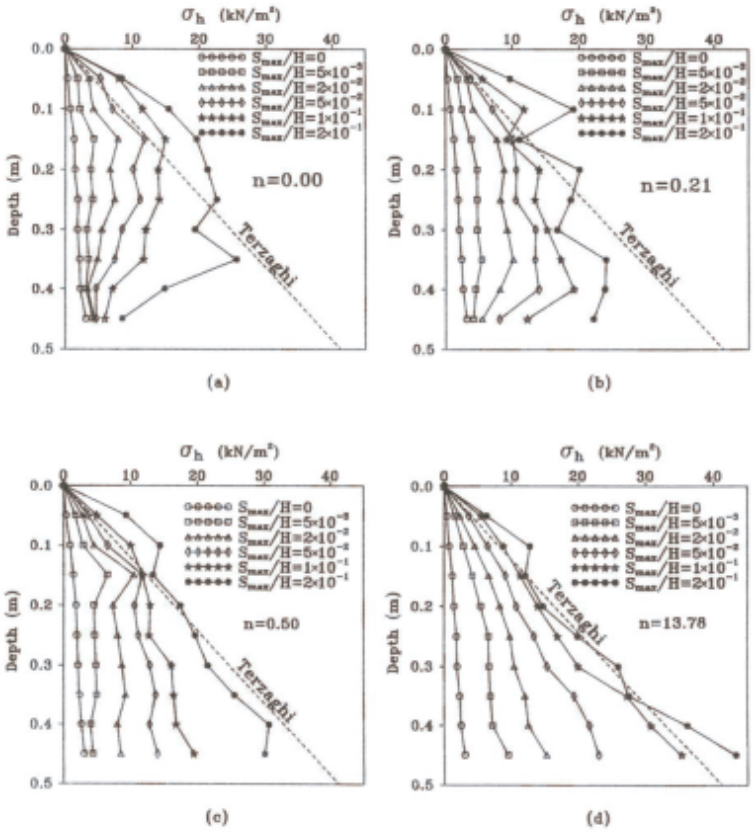

Figure 2.19. Distribution of horizontal earth pressure for RBT (rotation about a point below the wall base) mode (Fang *et al.*, 1994).

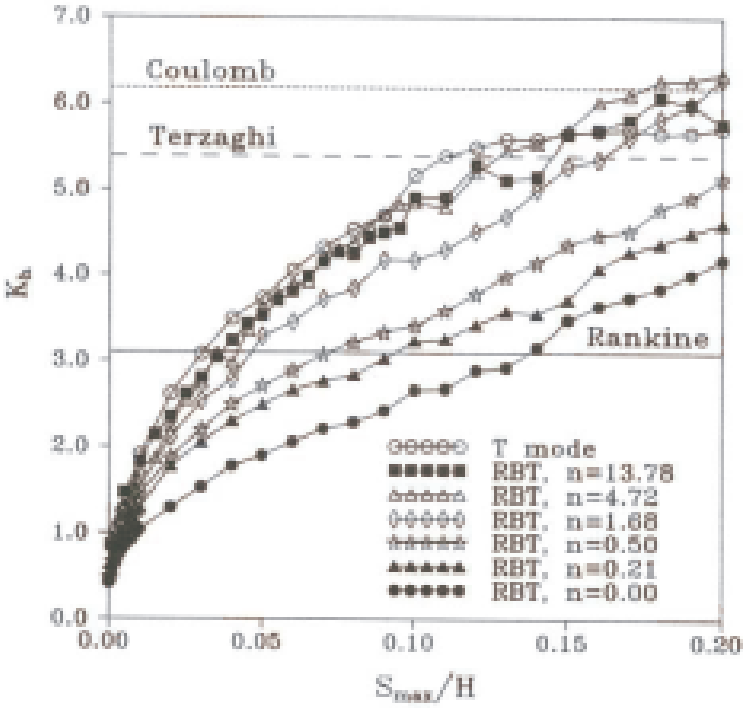

Figure 2.20. Variation of K_p with wall movement for RBT (rotation about a point below the wall base) mode (Fang et al. 1994).

Narain and Nandakkumaran (1969) asserted that the coefficient of passive earth pressure increased approximately linearly with the wall movement and the maximum values were reached at a wall displacement corresponding to 10% of the height of the wall for loose sand and 7.5% of the height of the wall for dense sand. According to Fang *et al.* (1994), an ultimate value for passive earth pressure coefficient K_P did not exist. Fang *et al.* (1994) found that soil pressures measured near the top increased with the increasing of wall movement. Narain and Nandakkumaran (1969) set up was similar as shown in Figure 2.21.

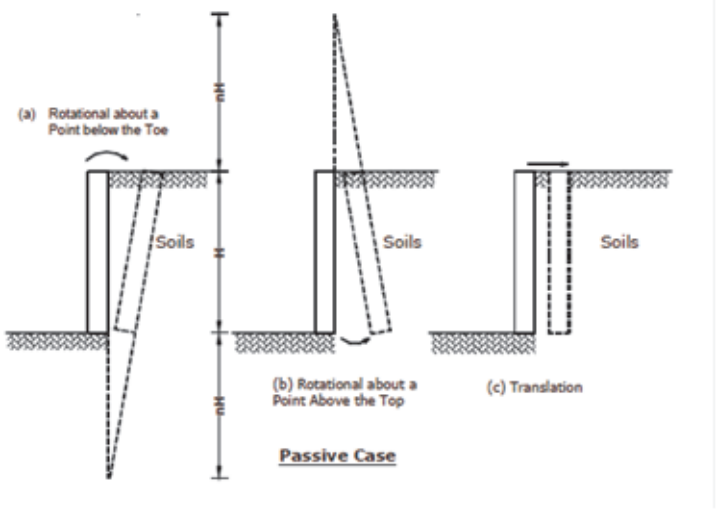

Figure 2.21. Passive wall movement modes (Fang et al., 1994).

Duncan and Mokwa (2001) claimed that the main drawback of the Coulomb Theory stems from the fact that it is assumed that the passive failure mechanism involves sliding along a plane surface. As a result, values of K_p computed using the Coulomb Theory is too high when the value of d is larger than about 0.4ϕ. As the value of δ approaches ϕ, the error in the Coulomb value of K_p becomes very large, as shown in Table 2.2.

Table 2.2. Comparison of K_p values computed by rankine, coulomb, and log spiral theories for level ground surface and $\phi = 40^o$ (Duncan and Mokwa 2001).

Wall friction (δ/ϕ) (1)	Rankine Theory (Kp) (2)	Coulomb Theory (Kp) (3)	Log Spiral Theory (Kp) (4)
0	NA	4.6	4.6
0.2	NA	6.3	6.6
0.4	NA	9.4	9.0
0.6	NA	15.3	11.9
0.8	NA	30.4	15.5
1	NA	92.6	17.5
Note: NA= not applicable.			

Duncan and Mokwa (2001) point out that the Log Spiral Theory uses the curved failure surface as shown in Figure 2.22. It results in smaller values of K_p than does the Coulomb Theory. They said that because of Coulomb and Log Spiral are upper-bound theories, the smaller the value of K_p, the more accurate it is. Thus the Log Spiral Theory is superior to the Coulomb Theory for conditions where δ exceeds 0.4ϕ.

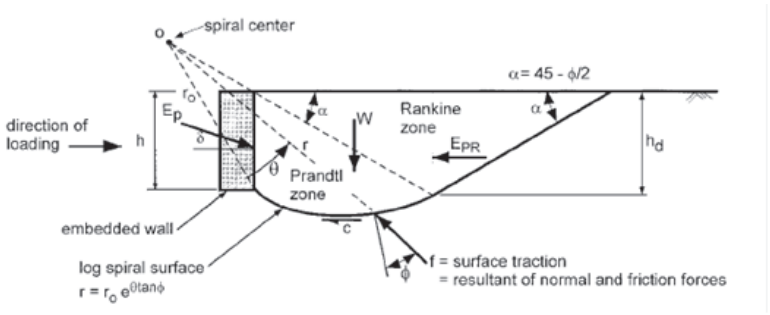

Figure 2.22. Log Spiral Failure Mechanism.

Duncan and Mokwa (2001) illustrated that the Log Spiral Theory can be used in three different ways. The simplest is to use tables or charts of passive pressure coefficients based on the Log Spiral Theory, which are found in Caquot and Kerisel (1948) and NAVFAC (1982). The limitations of these charts and tables are that they apply only to simple conditions and do not provide a means of accommodating the cohesive component of shear strength Duncan and Mokwa (2001). The second one is the graphical procedure, which requires time and effort, as explained in Terzaghi (1943) and Terzaghi *et al.* (1996). The third one is numerical analysis. Duncan and Mokwa (2001) have developed an Excel spreadsheet computer program called PYCAP that is based on the Log Spiral Theory. The spreadsheet is limited to vertical walls, horizontal ground surface, and uniform surcharge. In addition to the Log Spiral Theory, the spreadsheet includes the Ovesen-Brinch Hansen correction for 3D effects, making it applicable to short as well as long structures.

Duncan and Mokwa (2001) concluded that passive resistance to movement of structures is controlled by the amount and direction of movement of the structure, strength and stiffness of the soil, friction and adhesion on the interface between the soil and structure, and shape of the structure. They also pointed out that the shear

strength and elasticity parameters used in the calculations must reflect the behavior of the soil in the field, including density, drainage conditions, and range of confining pressure.

Hanna and Khoury (2005) performed an experimental investigation into the coefficient of passive earth pressure of overconsolidated homogeneous sand. Hanna and Khoury (2005) designed a prototype model of a vertical rough wall, retaining horizontal backfill in order to investigate the effect of stress history in the design theories for the passive earth pressure. They instrumented a modal in order to measure the total passive earth pressure acting on the wall, the passive earth pressure acting on selected locations on the wall, and the overconsolidation ratio (OCR) of the sand in the testing tank.

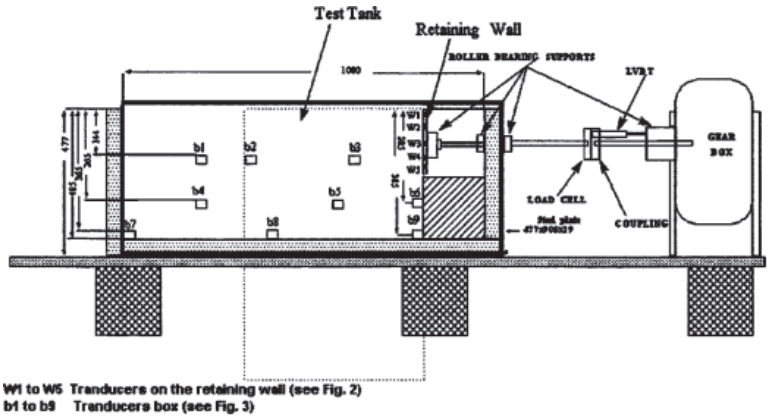

Figure 2.23. Layout of experimental setup (Hanna and Khoury, 2005).

Hanna and Khoury (2005) used well-graded sand for the investigation. Table 2.3 presents a summary of the properties of the sand. They used a direct shear box test in order to obtain the angles of shearing resistance, , of the sand and the angles of friction between the sandpaper and the sand. Hanna and Khoury (2005) used density cans to measure the unit weight of the sand in the testing tank. The sand was placed in layers 100 mm thick. A layer of 170 mm thick dead sand was placed at the bottom of the testing tank to reduce the effect of vibration reflection from the base. They compressed each layer using a hand air compactor with an end steel plate. Hanna and Khoury (2005) performed the tests by using homogeneous overconsolidated dense,

medium, or loose sands, overconsolidated dense sand backfill overlying medium sand deposit, and overconsolidated medium sand backfill overlying dense sand deposit.

Table 2.3. Summary of physical characteristics of sand (Hanna and Khoury 2005).

Property	Value
Classification	Well graded (SW-SC)
Description	99% silica
Shape of particles	Angular
Coefficient of uniformity (C_u)	10.93
Coefficient of curvature (C_c)	1.30
Specific gravity (G_s)	2.62
Maximum unit weight (γ_{max})	19.92kN/m
Minimum unit weight (γ_{min})	17.45kN/m
Maximum void ratio (e_{max})	0.52 (ASTM)
Minimum void ratio (e_{min})	0.33 (ASTM)

Hanna and Khoury (2005) obtained that compaction of backfill made of cohesionless material induces additional stresses in the backfill. They obtained failure surface for the case of overconsolidated backfill made of dense sand overlying medium sand deposit is given in Figure 2.24. It can be noted from this figure that the failure mechanism extends to the lower weak deposit. As a result, they suggested that the presence of the weak deposit below the founding level contributes to the value of the passive earth pressure acting on this wall. For the case of a strong overconsolidated cohesionless backfill overlying a weak deposit, the failure mechanism extends to the weak deposit, resulting in a significant reduction of the passive earth pressure acting on these walls. The observed failure surface for the case of overconsolidated backfill made of medium sand overlying dense sand deposit was given in Figure 2.24. They pointed out that the failure mechanism remained confined to the upper backfill layer; and further, the lower strong deposit does not contribute significantly to the passive earth pressure produced on the wall. For the case of a weak overconsolidated cohesionless backfill overlying a strong deposit, the failure mechanism does not extend to the strong deposit and remained confined to the backfill layer. Hanna and Khoury (2005) claimed that the

passive earth pressure on these walls can be calculated based on the condition of the backfill material, as the lower deposit does not influence the failure mechanism.

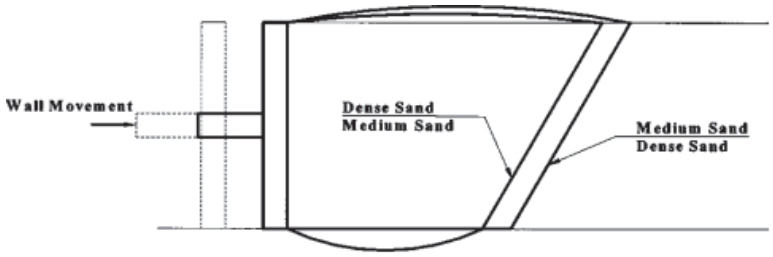

Figure 2.24. Experimental results-observed failure planes (Hanna and Khoury, 2005).

Fang and Lee (2006) investigated the influence of backfill densities on passive earth pressure. They conduct experiments with using vertical rigid wall, which moved toward a mass of dry sand. Air-pluviation method was used in their experiments. Fang and Lee (2006) concluded that for the wall with dense backfill, the earth pressure coefficient, K_p, increased with increasing wall movement. After reaching a peak value, K_p decreased with increasing wall movement, and finally reached an ultimate value. They point out that the Coulomb and Terzaghi solutions calculated with the peak angle significantly overestimated the ultimate passive trust. They also asserted that as the wall movement S/H exceeded 0.14, the passive soil trust would reach a constant value, regardless of the initial density of backfill in Figure 2.25. It may be deduced that, soils along the rupture surface had reached the critical state, and the shearing strength on the surface could be properly represented with the residual, ϕ_r, angle.

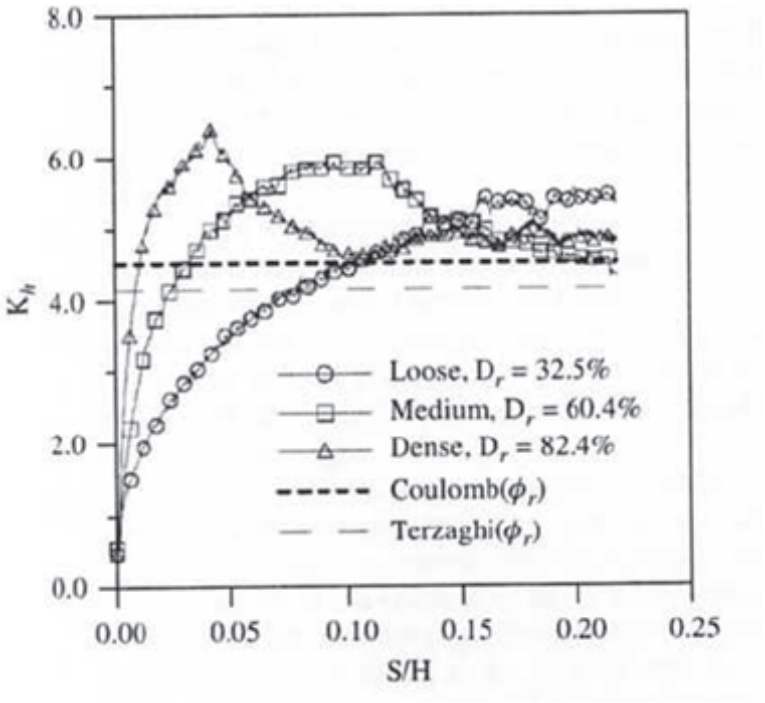

Figure 2.25. Variation of K_p with wall movement for loose, medium dense and dense backfill (Fang and Lee, 2006).

In addition to these, they claimed that for walls medium dense and dense backfill, Coulomb and Terzaghi solutions calculated with the peak friction angle, ϕ_{peak}, significantly overestimated the ultimate passive trust. However, if the residual friction angle, ϕ_r, was adopted to the Coulomb and Terzaghi theory, the theoretical solutions were obtained to be in relatively good agreement with the experimental ultimate trusts in Figure 2.26. They recommended that when calculating the passive earth pressure, the dilation and the strength reduction should be considered.

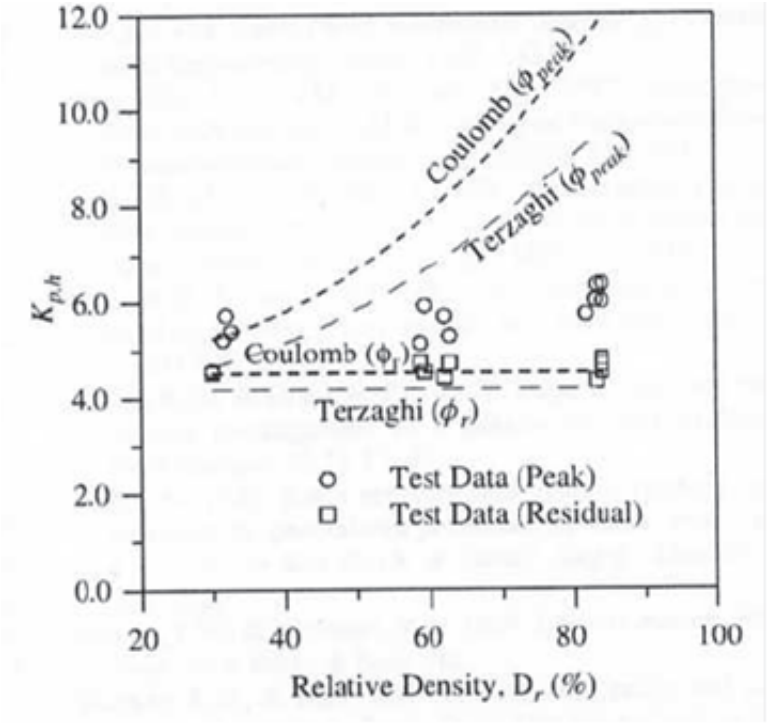

Figure 2.26. Variation of K_p, adopted with as a function of soil density (Fang and Lee, 2006).

Tejchman and Tantono (2007) focused on influence of initial density of cohesionless soil on evolution of passive earth pressure and the formation of shear zones in a dry sand body behind a retaining wall. They numerically investigated the evolution of shear localization, dilatancy and contractancy, micro-rotation and earth pressure behind a very rough and rigid retaining wall undergoing a horizontal translation against the backfill under plane strain condition using the finite element method and a micropolar hypoplastic continuum model. A micro-polar hypoplastic model takes into account stresses and couple stresses, pressure dependent limit void ratios and the mean grain size as a characteristic length. At the end of the investigation, they concluded that for the initially dense material, dilatancy develops during passive wall translation within the localized zones. At this point, dilatancy is accompanied with a reduction of the resulting earth pressure. However, the initially loose material was compacted during passive wall translation within the localized zone. They claimed that the maximum passive earth pressure strongly depends on the magnitude and distribution of the initial density, pressure level and mean grain diameter.

They concluded that the peak friction angle for an initially dense material and a low pressure level can be very high which leads to a high maximum earth pressure. After the peak, the earth pressure is reduced with continuous passive wall translation. For the initially loose material, the earth pressure increases during passive wall translation and shear localization takes place without a reduction of the resulting earth pressure. As a result of this, they illustrated that the global material softening is not always necessary to obtain shear localizations whose formation mainly depends on the boundary conditions of the entire system. They also asserted that the distribution of the initial void ratio slightly affects the geometry of shear zones.

2.3. Active Earth Pressure

Estimation of the active earth pressure has a significant role in the design of many geotechnical engineering structures, particularly retaining walls. For the calculation of active earth pressure, Coulomb's and Rankine's theories are commonly used. These theories assume that the distribution of active earth pressure exerted against the retaining wall is triangular as shown in Figure 2.27 and Figure 2.28.

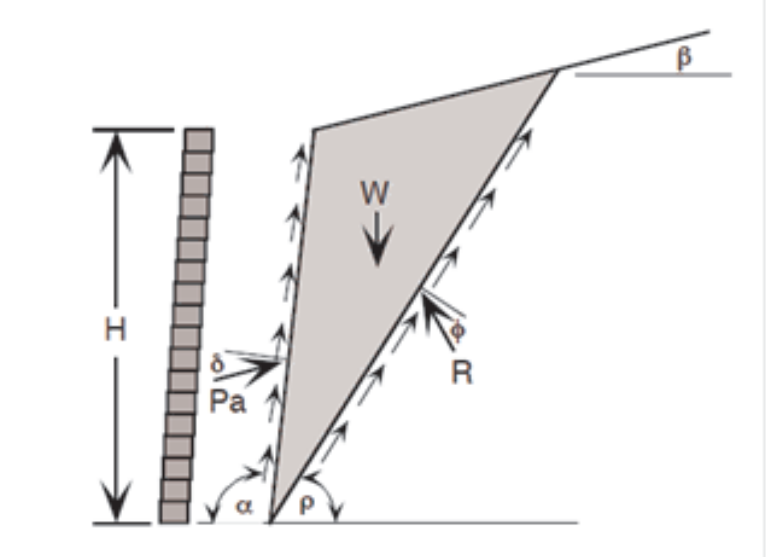

Figure 2.27. Coulomb analysis.

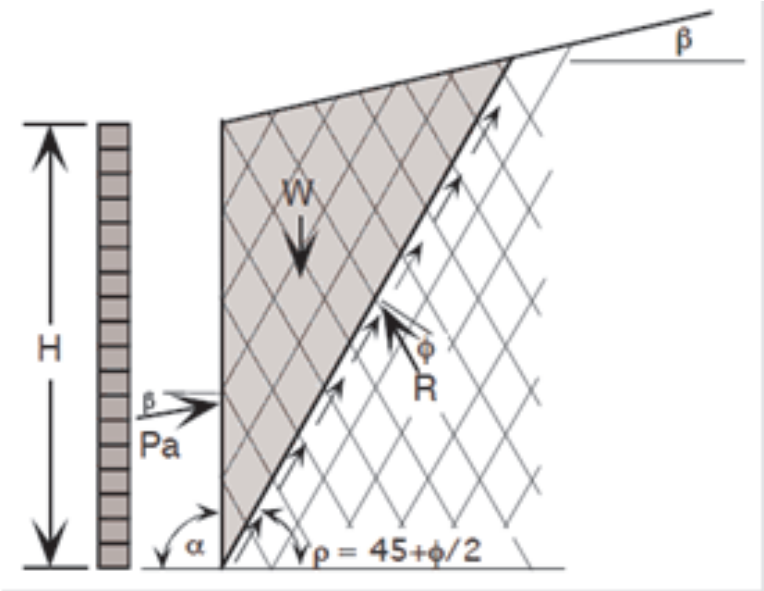

Figure 2.28. Rankine analysis.

However, many experimental results indicated that the active earth pressure distribution on a retaining wall is not triangular but nonlinear. In addition to this, Coulomb's and Rankine's formulas underestimate the height of the center of pressure. Some researchers have investigated the underlying reasons of this non-linearity and they tried to find the shape of slip surface, magnitude and height of application of lateral active force in retained soil mass.

Terzaghi (1936) conducted experiments to observe that the change in wall pressure from at-rest to active or passive state is a function of the wall movement. He asserted that the failure surface is approximately parabolic due to the arching effects. Arching is the stress redistribution process by which stress is transferred around a region of soil mass, which as a result reduces the stresses on the soil mass. A simple example of arching is what occurs in a large box of soil with a panel at the base. When this panel is lowered, the soil immediately above it will tend to move down with it as can be seen in Figure 2.29.

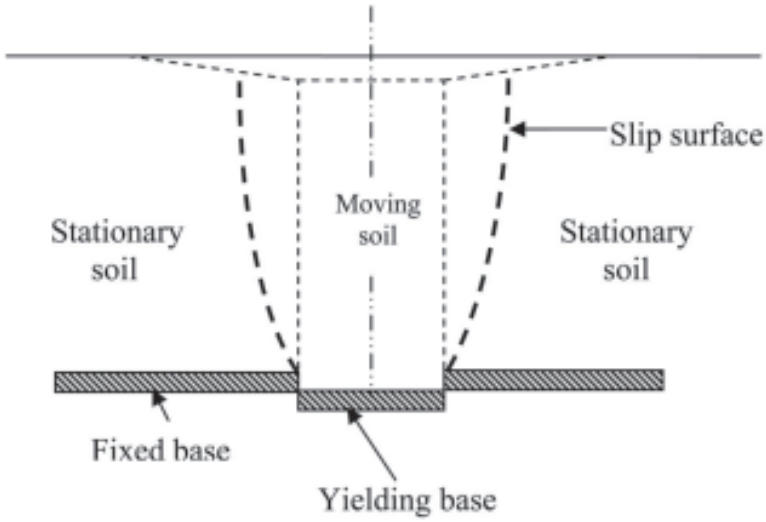

Figure 2.29. Stress redistribution caused by arching (Paik and Salgado, 2003).

Handy (1985) investigated the arch in soil arching. He explained that soil arching action develops in two stages: in the first stage rotation of the principal stresses adjacent to a rough wall and causes horizontal wall pressures to significantly exceed those from classical theory, simulating a K_o pressure distribution even in loose backfill soil. The second stage reduces pressures on the lower wall to give a curvilinear distribution typically centered at a height 0.42 times the height of the wall. To be more precise, he claimed that the first stage is rotation of principal stresses at the wall. That is because wall pressures appreciably higher than those predicted from Rankine or Coulomb analyses, and is essentially hydrostatic or triangular in distribution. At its maximum development, it approximately equals the Jaky expression for earth pressure at rest. This second stage of arching reduces vertical and horizontal pressures, particularly near the base of the wall. It yields a rounded pressure distribution rather than triangular pressure distribution, with the center of action about 0.4-0.45 times the height of the wall. In its second stage, arching action reduces wall pressures significantly below those from the Coulomb analysis, but places their center of action higher on the wall; the two effects are approximately compensatory for determining overturning moments. The curved pressure distribution from arching theory is relevant for calculation of shear and bending moments at various levels in the wall (Handy, 1985).

Fang and Ishibashi (1986) investigated the distribution of active earth pressure

against retaining wall rotating about its top. They use Ottawa sand as a backfill material. Based on the results, they indicated that the distribution of active earth pressure against retaining wall rotating about its top is nonlinear. They explained that the non-linearity results from the soil arching and the magnitude of the arching stress increased with increasing density of soil as shown in Figure 2.30.

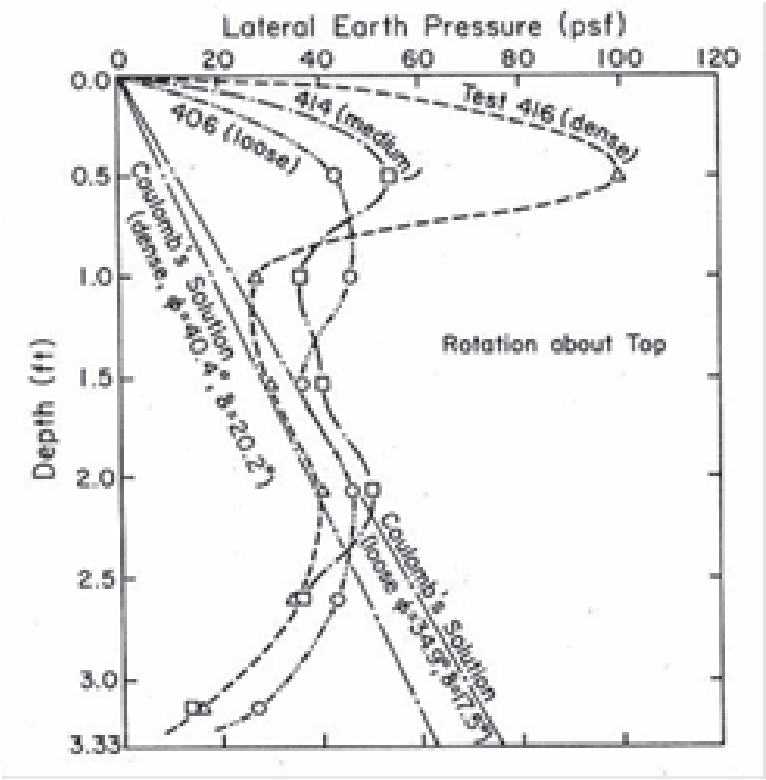

Figure 2.30. Distribution of horizontal earth pressure at active condition (rotation about top) (Fang and Ishibashi, 1986).

Fang and Ishibashi (1986) claimed that the arching zone extended downward from the top of the backfill to a depth ranging from one third to one fourth the height of the wall for the retaining wall rotating about its top. For rigid retaining walls considering translation mode, the lateral earth pressures measured at various depths decreases rapidly with wall movement until the active state was reached. After that, the lateral earth pressure did not change with further wall translation movements as shown in Figure 2.31.

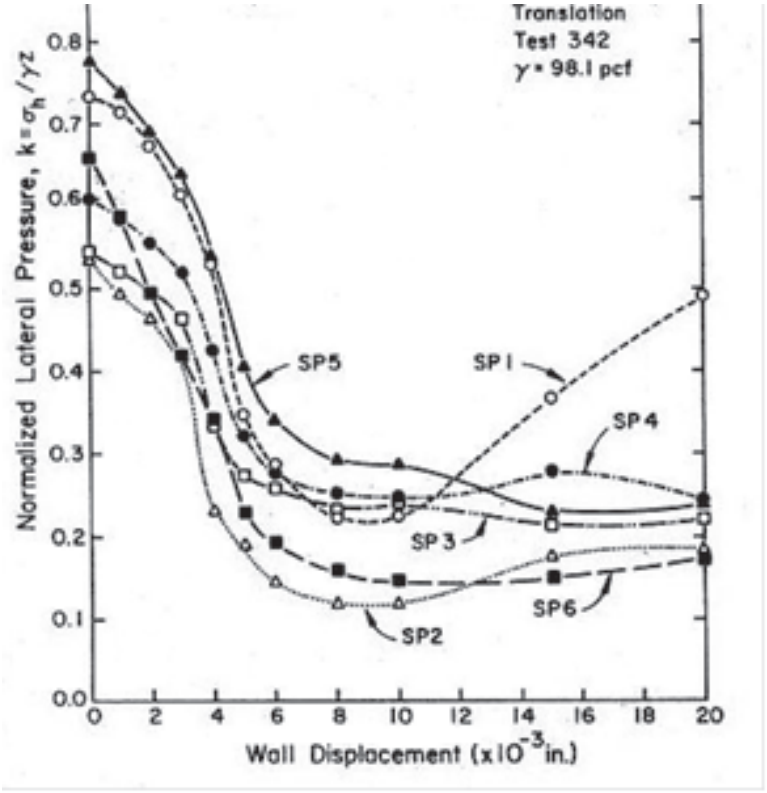

Figure 2.31. Change of normalized lateral pressure with translational wall displacement(Fang and Ishibashi, 1986).

Fang and Ishibashi (1986) suggested that for the wall rotating about base, the lateral pressure at the upper elevations decreased fast, whereas the lateral stress near the base of the wall decreased slowly with wall rotation as shown in Figure 2.32.

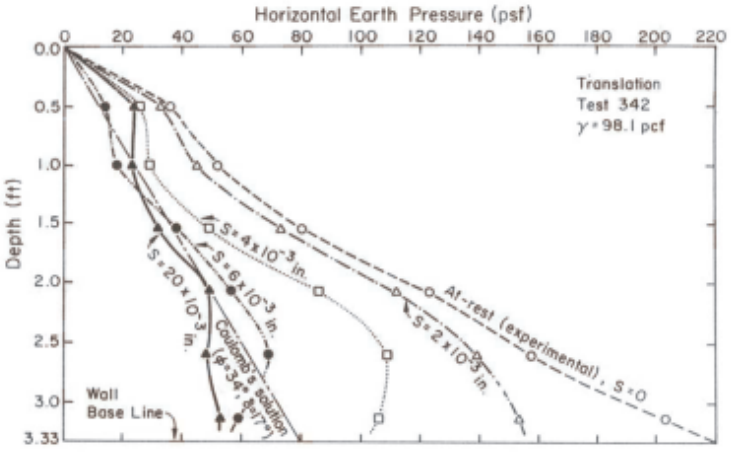

Figure 2.32. Distribution of horizontal earth pressure at different wall rotations (rotation about base) (Fang and Ishibashi, 1986).

Paik and Salgado (2003) considered the arching effects in the calculation of active earth pressure on a horizontally translating rigid wall. They tried to propose new formulation which accurately predicts both the earth pressure distribution and the lateral active force on the translating wall. Paik and Salgado (2003) illustrated that a rigid retaining wall may yield by either tilting or translating away from the backfill. The shape of the slip surface depends not only on wall friction angle, δ, but also on the yielding mode. They used Janssen (1985) arching theory to investigate the state of stress in the retained soil. They assumed two parallel rigid vertical walls retain granular soil, and that the settlement of the retained soil is large enough to fully induce friction between the walls and the soil. It follows that the weight of any differential flat element in the retained soil is partially supported by the frictional resistances at the walls, and the frictional resistances cause changes in the direction of the principal stresses acting on the differential element as shown in Figure 2.33. The major principal stresses on the differential flat element are applied normal to the concave arch represented by the dotted lines, while the minor principal stresses are tangential to the direction of the concave arch, becoming horizontal at the center of the element (Handy, 1985). Similarly, if a rigid retaining wall with a rough face moves away from the soil horizontally, the direction of the major and minor principal stresses on the differential flat element as shown in Figure 2.33 is changed owing to the frictional resistance at the wall (Paik and Salgado, 2003).

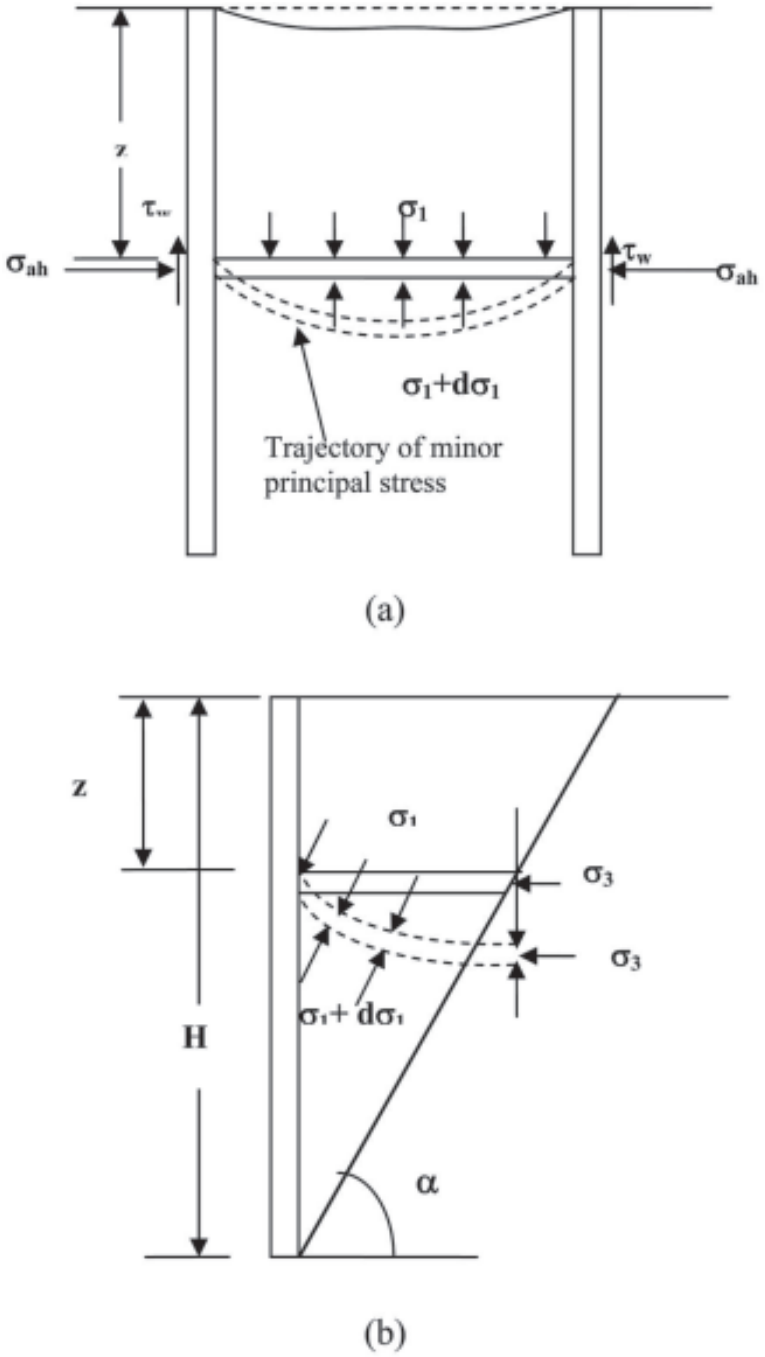

Figure 2.33. Trajectory of minor principal stresses: in granular fill at ditch; in backfill behind retaining wall (Paik and Salgado, 2003).

The minor principal stresses, σ_3, on the differential flat element behind the wall acted along the concave arch shown in Figure 2.34. However, the major principal stresses, σ_1, are perpendicular to the concave arch. Paik and Salgado (2003) used the Mohr circle to obtain the rotation angle, ϕ, of the principal stresses for the wall with

a wall friction angle of $\delta \leq \phi$ in Figure 2.34.

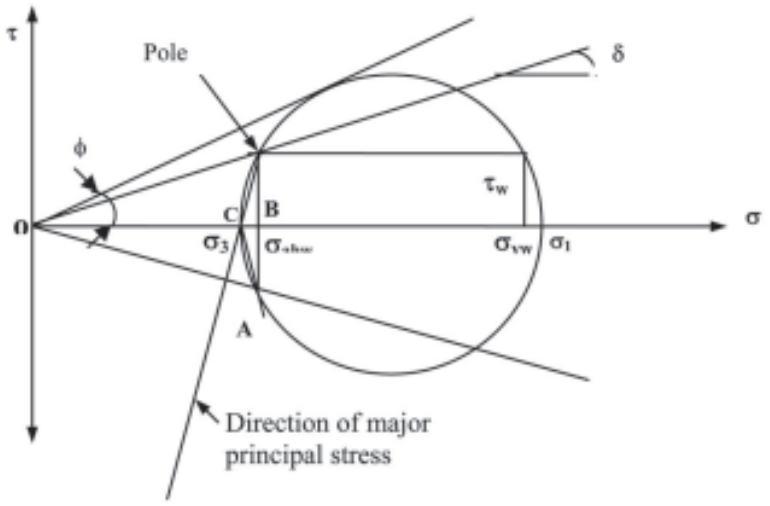

Figure 2.34. Mohr circle for stresses at wall (Paik and Salgado, 2003).

Paik and Salgado (2003) conducted parametric study to investigate the effect of friction angle, soil-wall interface friction angle and the height of wall. They obtained that the internal friction angle increases, the active earth pressure acting on the wall decreases at every depth. In addition to this, the height of the centroid of the active earth pressure distribution increase and the distance of the centroid of the active earth pressure distribution from the base of the wall increases with increasing soil-wall interface friction angle. Paik and Salgado (2003) also illustrated that the wall height does not have an effect on the shape of the active earth pressure distribution, but does have an effect on the magnitude of the lateral active force. They suggested that the ratio of the height of the point of application of the lateral active force to the wall height is independent of wall height for all formulations.

Paik and Salgado (2003) compare their results with experimental results. Tsagareli (1965) measured the distribution of the active earth pressures on translating rigid retaining walls with five different heights (2.0, 2.5, 3.0, 3.5, and 4.0 m). The unit weight of the backfill used in Tsagareli's full-scale tests was 17.65 kN/m^3, with δ and ϕ reported as equal to 37°. They also compare their results with the values of predicted by analyses of Coulomb (1776), Handy (1985), Harrop-Williams (1989). As a result, Paik and Salgado (2003) suggested that the distribution of active earth pressure behind the

wall is non-linear, and the earth pressure distribution differs depending on the mode of wall movement. This is due to arching effects in the retained soil, which results from the frictional resistance between the wall and the soil.

Goel and Patra (2008) made a study in order to investigate the change of active earth pressure distribution for rigid retaining walls considering the arching effects and also the shape of the critical failure surface. They used various configurations of shape of critical failure surface and arch shape, namely planar failure surface with a parabolic arch and parabolic failure surface with a parabolic arch. Based on their results, they claimed that planar failure surface with parabolic arch shape predicts closest to the experimental values.

2.4. Plane-Strain Concept

Plane strain condition corresponds to the state of deformation during which the material is free to deform in two-dimensions while its deformation is fixed in the third dimension. Generally for soil mechanics problems, plane-strain state corresponds to the deformation state of soils underlying structures that are much longer in one direction than the other two directions (i.e., behind long retaining wall or below strip footings). In other words, in the case of plane strain there are non-zero strain components in the xy plane. In this case, the normal stress in the direction normal to the xy plane may be determined from the stresses acting on the xy plane ($\sigma_{xx}, \sigma_{yy}, \sigma_{xy}$) through elastic stress-strain relationships. Figure 2.35 illustrates the stress and strain conditions in plane strain state. The plane strain state can be observed at several geotechnical structures such as retaining walls with lateral earth pressure, strip foundations, embankments as shown in Figure 2.35. Bishop (1966) defined the plain strain state as shown in Figure 2.36.

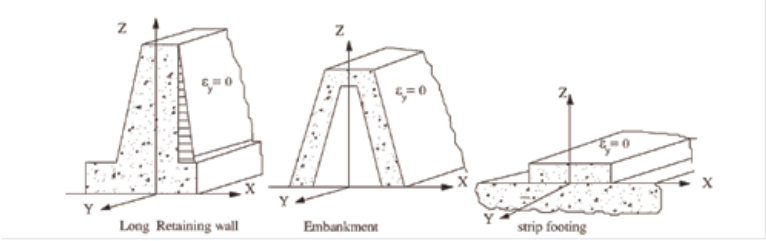

Figure 2.35. Geotechnical structures which are shown as an example of plane strain conditions.

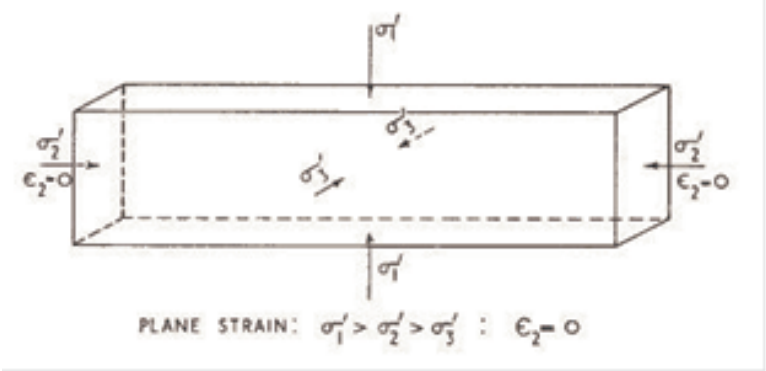

Figure 2.36. Plane-strain state: stresses and strains (Bishop, 1966).

Lee (1970) and Marachiet *et al.*, (1981) claimed that strength and deformation parameters of granular materials in plane-strain tests are different from those measured in triaxial tests. They also concluded that dense homogeneous sand tested under plane-strain conditions has higher shear strength and smaller strain at failure compared to conventional triaxial test results.

Vardoulakis (1977) suggested that the maximum angle of friction in triaxial test was 41^o whereas for the same sand and the same porosity the angle of friction of 47^o was measured in biaxial test.

Rowe (1969), Bolton (1986) and Vermeer (1990) asserted that both peak and critical friction angle is approximately the same in plane-strain and triaxial compression for very loose soils.

3. SELECTION OF THE SAND TYPE

Properties of the testing soil are directly influential on the possible outcomes of the experiments. That is why, in this chapter, the properties of the testing soil of choice will be described.

3.1. Sieve Analysis

This test method is used primarily to determine the grading of materials. The results are used to determine compliance of the particle size distribution with applicable specification requirements and to provide necessary data for control of the production of various aggregate products and mixtures containing aggregates. The data may also be useful in developing relationships concerning porosity and packing.

The sieve analysis is generally applied to the soil fraction larger than 75 μm. Grains smaller than 75 μm are sorted by using sedimentation (e.g., hydrometer or pipette analysis). Sieving can be performed in either wet or dry conditions. Dry sieving is used only for soils with a negligible amount of plastic fines, such as gravels and clean sands, whereas wet sieving is applied to soils with plastic fines. In the experiment, dry sieving method is used to obtain the grading of material. The grading of materials is determined following (ASTM D422-63, 2007) Standard Test Method for Particle-Size Analysis of Soils.

3.1.1. The Equipment Used in Sieve Analysis

For conducted sieve analysis the following equipment is used:

- Series of standard sieves with openings ranging from 7.5 cm to 75 μm, including a cover plate and bottom pan. Only a few sieves in Table 3.1 are selected for the sieve analysis.
- Oven

- Mechanical sieve shaker
- A balance sensitive up to 0.1 g.
- Soft wire brush.

Table 3.1. Sieve sizes used for the experiment.

Sieve Number	Size (mm)
# 4	4.75
# 16	1.18
# 20	0.85
# 30	0.6
# 40	0.425
# 50	0.3
# 70	0.212
# 100	0.15
# 200	0.075

3.1.2. Testing Procedure

There are two different procedures for dry and wet sieving. Dry sieving is used to obtain the grain size distribution curve. The following procedure is used for dry sieving analysis.

The laboratory book of Bardet (1997), Experimental Soil Mechanics is used as a main reference for the procedure of sieve analysis:

(i) The sample was dried and allowed it to cool. After that measured its weight.

(ii) The sieves were arranged. The largest mesh opening was at the top and the smallest was at the bottom.

(iii) A pan was attached at the bottom of the sieve stack. The sample was poured on the top sieve. A cover plate was used to avoid dust and loss of particles while shaking.

(iv) The stacks of sieves were placed in the mechanical shaker and shaked for about

10 min. Then the stacks of sieves were removed from the shaker. The weight of the soil which is retained in the sieves was recorded.

(v) After these steps, particle grain size distribution curve graph was drawn with the help of Excel Program.

3.1.3. The Result of Sieve Analysis

The experimental results are shown in Table 3.2 and particle size distribution graph can be seen from Figure 3.1.

Table 3.2. Sieve analysis calculation.

Sieve Number	Size (mm)	Sand + Sieve	Sieve	Weight Retained	Cumulative weight retained	Cumulative Retained	Percent Finer
# 4	4.75	410.46	410.46	0	0	0	1
# 16	1.18	425.4	424.86	0.54	0.08%	0.08%	99.92%
# 20	0.85	418.34	417.89	0.45	0.06%	0.14%	99.86%
# 30	0.6	410.26	406.85	3.41	0.49%	0.63%	99.37%
# 40	0.425	399.71	384.62	15.09	2.16%	2.79%	97.21%
# 50	0.3	445.73	374	71.73	10.25%	13.04%	86.96%
# 70	0.212	941.3	378.2	563.1	80.47%	93.51%	6.49%
# 100	0.15	429.56	389.05	40.51	5.79%	99.29%	0.71%
# 200	0.075	369.8	366.06	3.74	0.53%	99.83%	0.17%
PAN		416.08	414.88	1.2	0.17%	100.00%	0.00%
Total				699.77	100.00%		

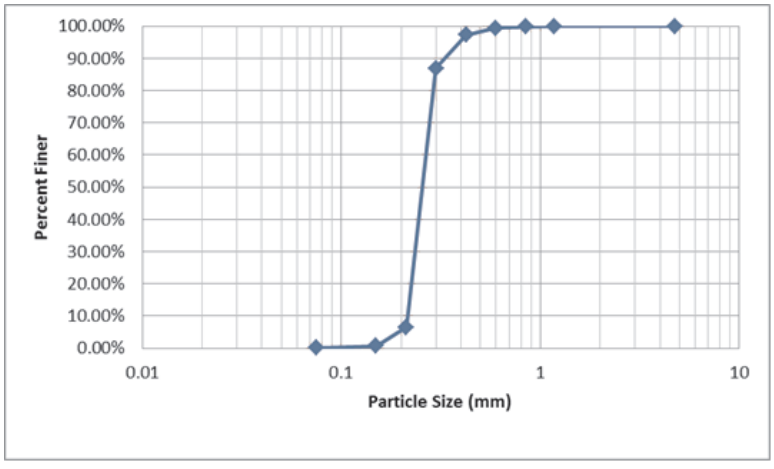

Figure 3.1. Particle size distrubition of sand.

3.1.4. Classification of Soils

Grain size distribution curves enable sand and gravels to be classified in three main types: uniform, well graded, and poorly graded.

3.1.4.1. Uniformly Graded Soils. In uniform soils, the majority of grains are nearly the same size. The uniformity in soils is characterized by the uniformity coefficient C_u.

$$C_u = \frac{D_{60}}{D_{10}} \tag{3.1}$$

where D_{10} is the grain size corresponding to 10% finer and D_{60} is the grain size corresponding to 60% finer. represents the average slope of the grain size distribution between 10 and 60%. The smallest possible value for C_u is equal to 1 and corresponds to a perfectly uniform assemblage of grains of identical size.

3.1.4.2. Poorly-Graded Soils. The term poorly graded applies to any soil, including uniform soil, which does not comply with the description of well graded. Poorly graded soils are deficient in certain sizes. Gap-graded materials are examples of poorly graded materials with missing ranges of particle sizes. In practice, gap-graded materials are generally found in the coarse sand, fine gravel range.

The sand used in the experiment can be classified as a uniformly graded soil considering the sieve analysis results as shown in Table 3.3.

Table 3.3. Classification of soils.

Uniformity coefficient (Cu)	D60	D30	D10 (effective size)
1.23	0.27	0.24	0.22
Coefficient of gradation (Cc)			
0.97	0.67	0.24	0.22

3.2. Determination of Specific Gravity

Specific gravity is the ratio of the mass of unit volume of soil to the mass of the same volume of gas-free distilled water. The significance of the determination of specific gravity is that the specific gravity of a soil is used in the phase relationship of air, water, and solids in a given volume of the soil.

The specific gravity of soil solids is determined following the ASTM standard D854, Standard Test Methods for Specific Gravity of Soil Solids by Water Pycnometers. The test method covers the determination of the specific gravity of soil solids that pass the 4.75 mm (No. 4) sieve, by means of water pycnometer. Method B procedure from ASTM D854 is appropriate for oven dried specimens, thus it is used in the experiment.

3.2.1. The Equipments Used in Specific Gravity Analysis

The equipment for determination of specific gravity included:

- Volumetric flasks 500 mL with stoppers numbered and calibrated.
- Vacuum pump.
- Balance accurate to 0.01 g.
- Distilled deaired water.
- Thermometer, ranging from 0 to 50 ^{o}C accurate to 0.5 ^{o}C.
- Drying oven.
- Evaporating dish.

3.2.2. Test Procedure

The laboratory book of Bardet (1997), Experimental Soil Mechanics is used as a main reference in this section.

(i) The samples were taken approximately 100 g of air-dried soil. Due to the fine-grained soil used for the experiment, the sample was mixed with water in an

evaporating dish to make about 200 ml. of soil-water mixture.

(ii) The soil-water mixture was transferred from the evaporating dish into the volumetric flask. Then the flask was washed in order to prevent any remaining soil in the flask. After that water was added to fill the flask two-thirds to three-fourths full. It was not filled completely, because its contents must be agitated under vacuum.

(iii) The vacuum lines attached to the flask and for at least 10 min gently agitated the mixture. The reduced air pressure caused the water to boil.

(iv) When the de-airing process was completed, deaired water added to fill the calibrated flask volume.

(v) The weight of the flask measured and also the water temperature was measured.

(vi) The weight of soil which was dried in the oven was measured.

(vii) The test was repeated to calculate additional values of G_s until the values of G_s were within 2% of each other.

3.2.3. Data Analysis

The specific gravity of the soil solids calculated using the following formula:

$$G_s = \frac{W_s}{W_s + W_{fw} - W_{fs}} \tag{3.2}$$

Where W_s is the weight of the dry soil, W_{fs} the weight of the flask filled with soil and water, and W_{fw} the weight of the flask filled with de-aired water only.

For the determination of specific gravity three tests are conducted and the average is used. The specific gravity analysis results are summarized in Table 3.4.

3.3. Direct Shear Test

The direct shear simulates the effects of shear loads acting on a predetermined failure surface. The direct shear test is used to measure the friction angle, cohesion, and undrained shear strength of soils for stability analysis of foundations, slopes, and

Table 3.4. Specific gravity results.

Soil	Specific Gravity
Sample 1	2.61
Sample 2	2.62
Sample 3	2.65
Average	2.63

retaining walls.

Direct shear test is used to obtain the angles of shearing resistance, ϕ, of the sand in the experiment. The shearing resistance is determined following the ASTM standard, D3080 - 04 Standard Test Method for Direct Shear Test of Soils Under Consolidated Drained Conditions.

3.3.1. The Equipment Used in the Direct Shear Test

- Direct shear loading machine with a counterbalance system for the application of normal load.
- Direct shear box.
- Assortment of slotted weights for applying the normal load.
- Two dial gages for measuring vertical and horizontal displacements sensitive to 0.01 mm with a full range of 2.5 cm.
- One calibrated load ring for measuring the shear force. A capacity of 2 kN is suitable for most purposes.
- A larger capacity (e.g. 5 or 10 kN) may be required for larger normal loads. The load ring may be replaced by a load transducer of similar range.
- A 2.5-cm ball bearing for applying the normal load to the sample cap.
- Tamper for compacting cohesionless soil.
- Balance, sensitive to 0.l g.
- Timer and calipers.
- Spoons and straightedge.

3.3.2. Test Procedure

There are two different tests -procedures, depending on whether the soil to be tested is coarse grained or fine gained. The procedure for the coarse grained is appropriate for sand which is used in the experiment.

The laboratory book of Bardet (1997), Experimental Soil Mechanics is used as a main reference in this section.

(i) The internal side length for square cell was measured.
(ii) The counterweight system calibrated so that it applies a small but negligible normal force.
(iii) The cap was weighted.
(iv) The direct shear box assembled and mounted it on the direct shear machine. The mounting pins were inserted to align the upper and lower parts of the direct shear box.
(v) The gap between the two parts of the shear box adjusted by turning the setscrews. In theory, the spacing should be larger than the diameter of the largest particle to prevent the top part from riding up on the grains that get caught in the gap. In practice, a spacing of approximately 0.5 mm is satisfactory.
(vi) The depth H_2 of the shear box and the height H_3 of the top cap were measured.
(vii) The dish filled with the sand to be tested was weighted.
(viii) While the pins hold the two parts of the shear box together, the sand was poured slowly to obtain a loose specimen. The sand was compacted with a tamper to obtain denser specimens.

3.3.3. Data Analysis

For the determination of the friction angle, cohesion, and undrained shear strength of soils four direct shear tests are conducted. The results obtained from direct shear apparatus is illustrated in Figure 3.2. From these results, the peak friction angle is obtained 32^o and cohesion 12kPa.

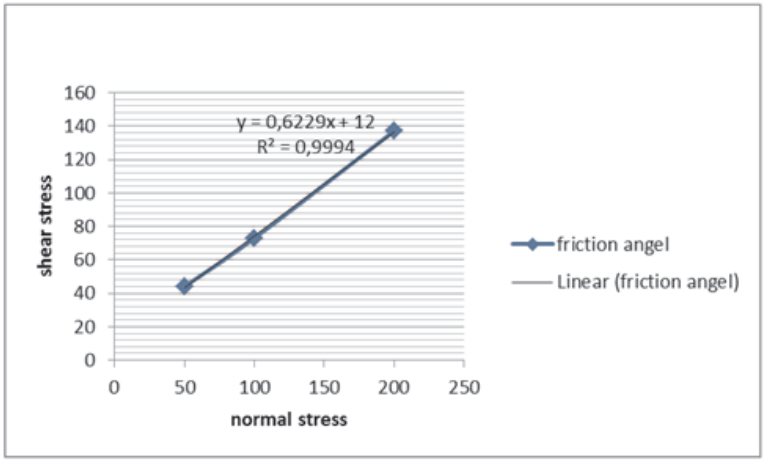

Figure 3.2. Direct shear test results.

3.4. Determination of Minimum and Maximum Index Densities

This test is conducted to determine the relative density of cohesionless soils using a vibrating table. The relative density of a soil is the ratio, expressed as a percentage, of the difference between the maximum index void ratio and the field void ratio of a cohesionless, free-draining soil; to the difference between its maximum and minimum index void ratios.

Relative density is used for evaluating the state of compactness of a given soil mass. The engineering properties, such as shear strength, compressibility or permeability, of a given soil depend on the minimum and maximum index densities.

The shearing resistance is determined following the ASTM standard, ASTM D 4254- Standard Test Methods for Minimum Index Density and Unit Weight of Soils and Calculation of Relative Density and ASTM D 4253 - Standard Test Methods for Maximum Index Density and Unit Weight of Soils Using a Vibratory Table.

3.4.1. The Equipments Used for the Determination of Minimum and Maximum Index Densities

The equipment for determination of minimum and maximum index densities included:

- Vibrating Table.
- Mold Assembly consisting of standard mold.
- Guide sleeves.
- Surcharge base-plate.
- Surcharge weights.
- Surcharge base-plate handle.
- Dial-indicator gage.
- Balance.
- Straightedge.
- Scoop.

3.4.2. Test Procedure of Minimum and Maximum Index Densities

(i) The mold was filled with the soil as loosely as possible by pouring the soil using a pouring device (funnel).

(ii) The soil surface was trimming with a straightedge.

(iii) The mass of the mold and soil were determined and recorded. Then empty the mold.

(iv) Again the mold was filled with soil with funnel. The sides of the mold was struck a few times using a rubber hammer to settle the soil so that the surcharge base-plate could be easily placed into position and there was no surge of air from the mold when vibration was initiated.

(v) The surcharge base plate was placed on the surface of the soil and twisted it slightly several times so that it was placed uniformly in contact with the surface of the soil. After that the surcharge base-plate handle was removed.

(vi) The mold was attached on the vibrating table.

(vii) Six sets of dial indicator readings were obtained from each side. The average of these twelve readings was the initial dial gage reading. These readings were recorded.

(viii) The guide sleeve was attached to the mold and the appropriate surcharge was weighted onto the surcharge base-plate.

(ix) The mold assembly and soil specimen was vibrated for 8 min.

(x) The dial indicator gage readings were obtained. The average of these readings was the final dial gage reading.

(xi) The surcharge base-plate was removed from the mold and detached the mold from the vibrating table.

(xii) The mass of the mold and soil were determined and recorded.

(xiii) The mold was emptied and determined the weight of the mold.

(xiv) The dimensions of the mold was determined and recorded in order to calculate the calibrated volume of the mold. In addition to that, the thickness of the surcharge base-plate was determined.

3.4.3. Data Analysis

For the determination of the minimum and maximum index densities, index densities test was performed. At the end of the test, e_{min} and e_{max} were obtained, respectively 0.58 and 0.79.

4. DESIGNING OF THE PHYSICAL MODEL

In this chapter the physical model is described in detail. The problems faced during the design, construction and testing stages are explained and the applied solutions are given.

4.1. The Physical Model

4.1.1. General Properties of the Physical Model

The model is designed in order to measure the passive and active earth pressures acting on the retaining wall. The physical model consists of a testing tank, a retaining wall model, a sand placing system, storage tank, crane and and the software. The schematic view of the physical model used in the present investigation is shown in Figure 4.1. The sides of the testing tank are plexiglass allowing the observation of deformations during testing. This way the deformations can be recorded for later analysis. Visual analyses of the tests will be conducted using particle image velocimetry (PIV) method. An aluminium plate capable of lateral translation simulates the retaining wall. The plate is equipped with five pressure transducers. The magnitude of the lateral thrust required for the translation of the plate is measured via a load cell. The wall moves either in forward or backward direction. To be more precise, the wall moves horizontally towards to backfill or vice versa without any rotation. Dry-pluviation is used in order to achieve desired relative density in the backfill material. The system is equipped with a storage tank for storing the test. A specifically designed mobile crane is used to transfer the sand from and to the storage tank. The crane is mobile and independent of the testing system which provides it with flexibility so that it can be used for other purposes within the laboratory. LabVIEW, a system design software, is used as the data acquisition system and also as the software interface. In order to observe the effect of friction between the wall and backfill, different stick-on materials will be used to develop a rough surface on the wall face. The properties of the device are explained in detail in the next sections.

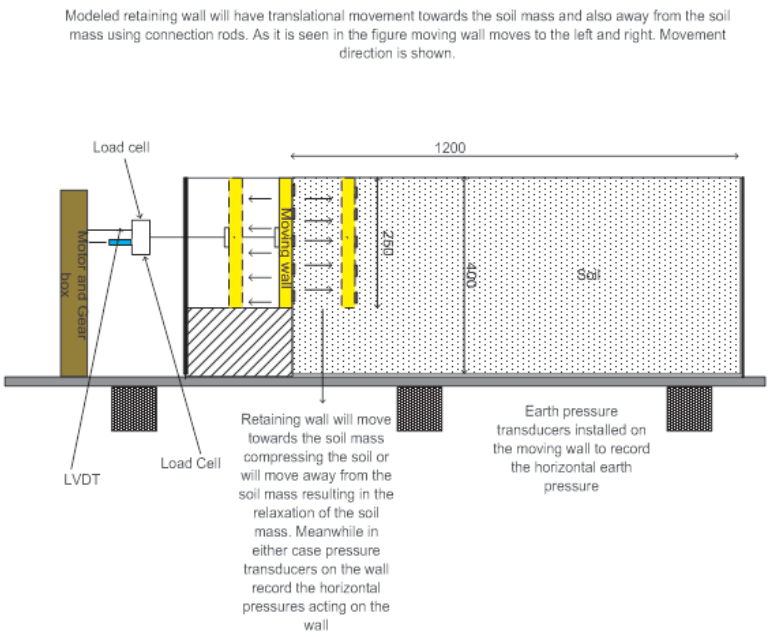

Figure 4.1. Schematic view of the physical modelSchematic view of the physical model.

4.1.1.1. Plane Strain Concept. Based on the literature survey, it could be decided that plane-strain state is an appropriate simplification of reality for understanding the behavior of backfill soils of retaining walls. As a result, our model will simulate stress and strain state observed behind long retaining walls. Accordingly, since the strength and deformation parameters of granular materials under plane-strain conditions are different from those measured in triaxial tests, the results obtained from the model will supplement the experimental data on lateral earth pressures obtained under axisymmetric conditions using the triaxial apparatus. Moreover, it would be possible to compare the influences of plane-strain behavior and axisymmetry state on the behavior of granular materials. Hence, the retaining wall model is designed with a width that is equal to the width of the tasting tank so as to provide plane strain condition. Dimension of the model is 140 cm, 60 cm, 50 cm in length, depth and width, respectively.

4.1.1.2. The Electronics. The model box has a moving aluminum plate that is simulating a retaining wall. The wall displacement is limited to only translation. In order

to minimize boundary effects, moving plate is designed 15 cm above the bottom.The retaining wall has a rectangular crosssection that is 35 cm high, 50 cm wide.Five pressure transducers are located on the face of the wall and a load cell is connected to the thrusting shaft that transmits the load for translation. In addition to these, two pressure sensors are located in the sand mass in order to measure the vertical effective stress at different depths. The load cell is connected to the back face of the wall as illustrated in Figure in order to measure the horizontal thrust that is required for movement of the wall. The type of the load cell is tension-compression cell that is stainless steel and its capacity is 5 kN. At the same location, the electronic ruler is placed to measure the displacement of the wall so that the displacement of the wall can be controlled and recorded for later use during the data analysis stage.

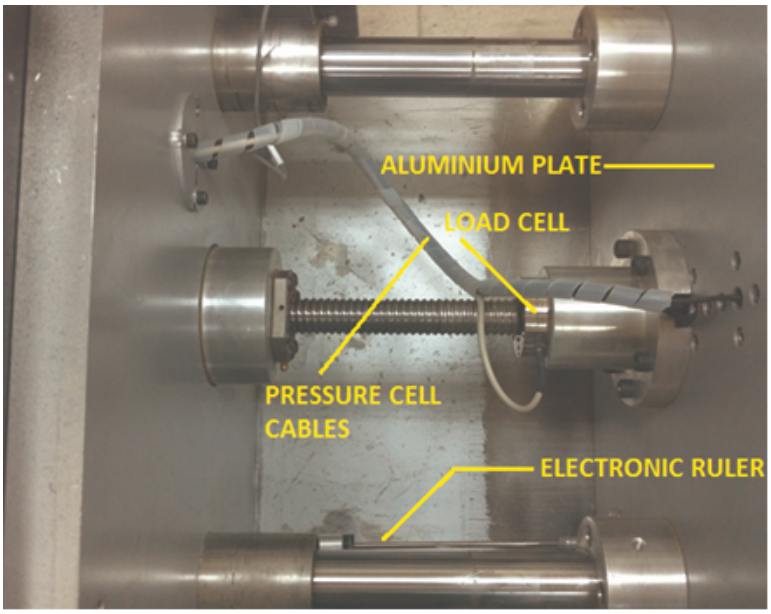

Figure 4.2. The back face of the retaining wall.

The vertical positions of the pressure transducers on the face of the model wall provide the means to monitor the variation of lateral earth pressure along the face of the wall during wall movement. These pressure transducers are installed at equally spaced intervals and they are aligned along the vertical centerline of the wal as illustrated in Figure 4.2. The capacity of the pressure transducers are 200 kPa and their specification is shown in Table 4.1. The pressure transducers used in the model have a high sensitivity, high stiffness and are insensitive to temperature variations.

Table 4.1. The specification of pressure transducers.

Type	KDE-200KPA KDF-200KPA
Capacity	200kPa
Rated output Approx.	0.3mV/V (600×10−6 strain)
Non-linearity	2%RO
Temperature range	$-20\sim +60\ ^oC$
Input/output resistance	350Ω
Recommended exciting voltage	Less than 3V
Allowable exciting voltage	10V
Cable drawing direction	KDE-PA : from side of body/KDF-PA : from back of body
Weight	160g

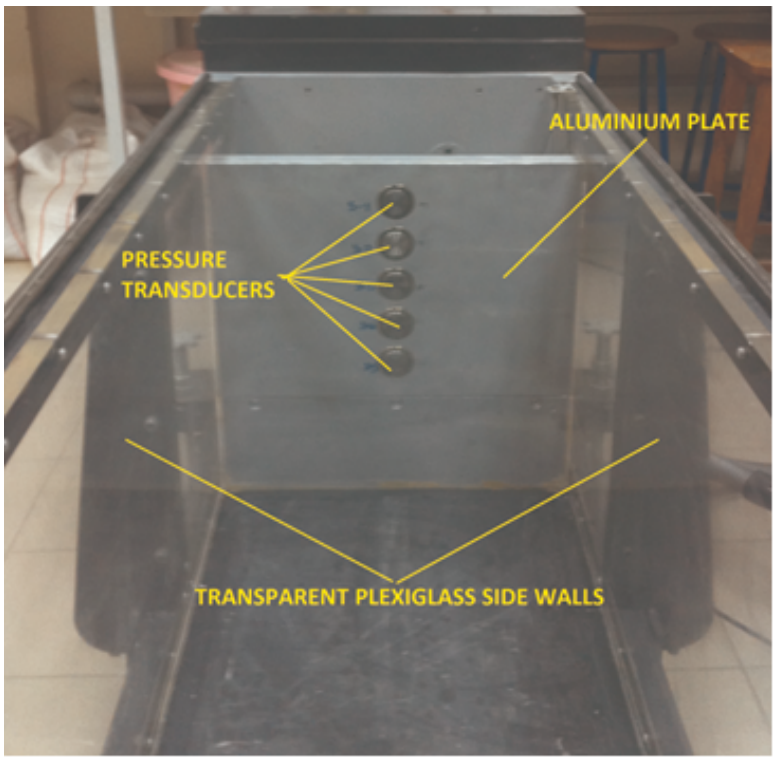

Figure 4.3. The location of pressure transducers and transparent side walls.

4.1.1.3. Obtaining the Data Coming from the Transducers. Initially, for data acquisition the circuit board shown inFigure was used. However unfortunately, it is noticed that the acquired data using this setup was low quality and not accurate. Some verification experiments were conducted in order to identify the source of the problem. At the end of these experiments, it could be understood that the capacity of the cir-

cuit board was not sufficient for measuring the data from the highly sensitive pressure transducers. Therefore, it is decided that the system should be changed.

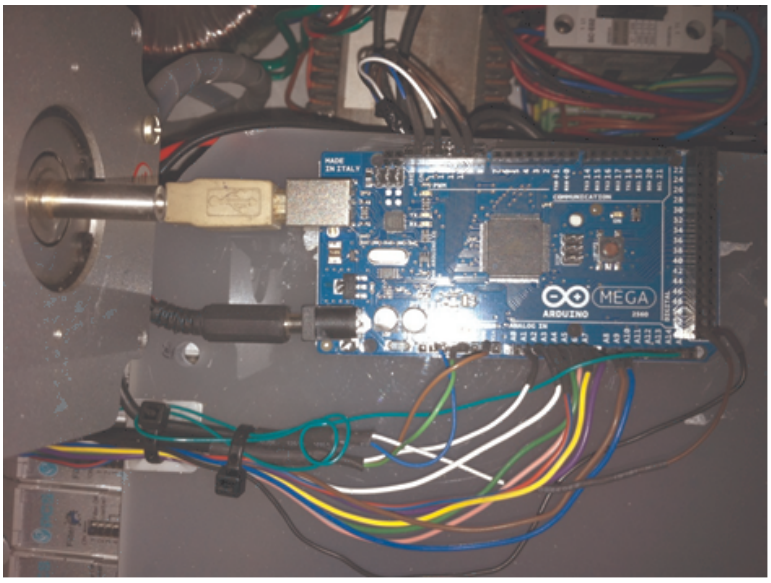

Figure 4.4. The circuit board of the electronic system.

In order to improve the capability of the measurement system, widely used system design software LabVIEW is used to convert the analog data to digital. LabVIEW provides engineers and scientists with the tools needed to create and deploy measurement and control systems through unprecedented hardware integration. LabVIEW software is also complemented with a data acquisition system consisting of nine channels as shown in Figure 4.5. The software program is created using LabVIEW to obtain the readings coming from the measuring devices in an automatic mode at predetermined intervals. A filtering program is added to the software in order to reduce the voltage noise, thus the sensitivity is improved. Each transducer has a unique calibration factor which is given in the manufacturer's guidelines. That is why, the calibration factor for each transducer is individually entered in the LabVIEW system. Moreover, the computer program allows calibrating the transducers individually using the manual mode.The transducers should also be separately calibrated before testing.

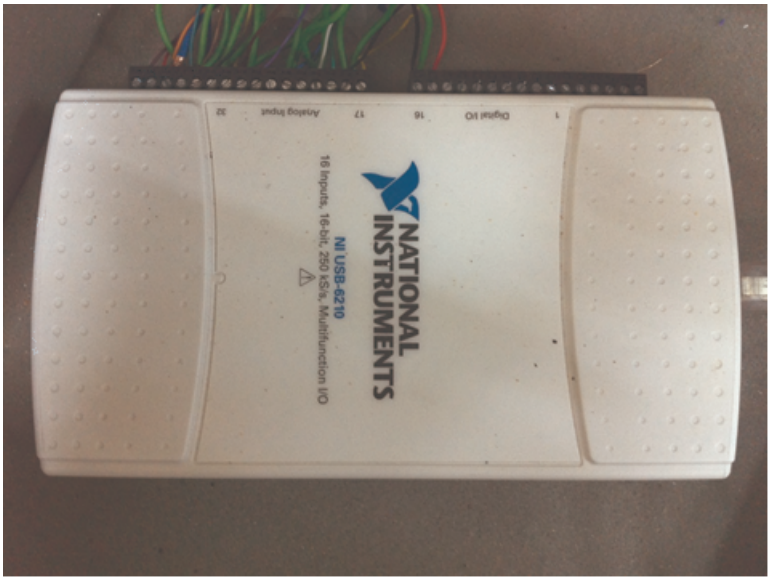

Figure 4.5. The data acquisition system of LabVIEW.

4.1.1.4. Sand Pluviation method. A special automatic pluviation device is designed in order to obtain the desired relative density. This device allows controlling the amount of flow and varying the speed of the device along the length of the model. A depiction ofthe pluviation device is shown in Figure 4.6.

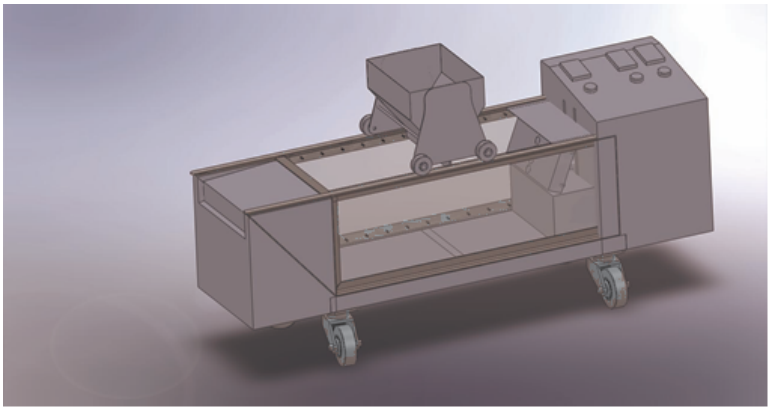

Figure 4.6. The drawing of the automatic pluviation device.

However unfortunately, the gap of the device through which the sand is poured could not be adjusted to the desired opening size. Because of this complication, it is decided that the pluviation device was not good enough to provide sufficient uniformity to the backfill soil. As a result, a new sand placement setup is devised which is simply

a funnel and a pipe system as shown in Figure 4.7. The new sand pluviation method is practical, simple, adjustable and and provides the researcher with the much needed control over the uniformity and density of the backfill soil.

Figure 4.7. The new pluviation system.

Density cans are used to measure the unit weight of the sand in the testing tank and placed in a staggered scheme in the vertical direction. The density cans measure is 54 and 34 mm in diameter and depth, respectively. These cans are taken out and weighted carefully. Using the measured data, the unit weight of the backfill sand is calculated from which the relative density is calculated

During the experiments, another cause for concern was the leakage of sand grains from the gaps between the side of the retaining wall plate and the plexiglass side wall. This problem was solved by attaching soft membrane sheets to the edges of the retaining wall plate. As the plate moves, the sheet closes the gap and prevents any

leakage. The material used for sealing the gaps and its application prior to a test is shown in Figure 4.8.

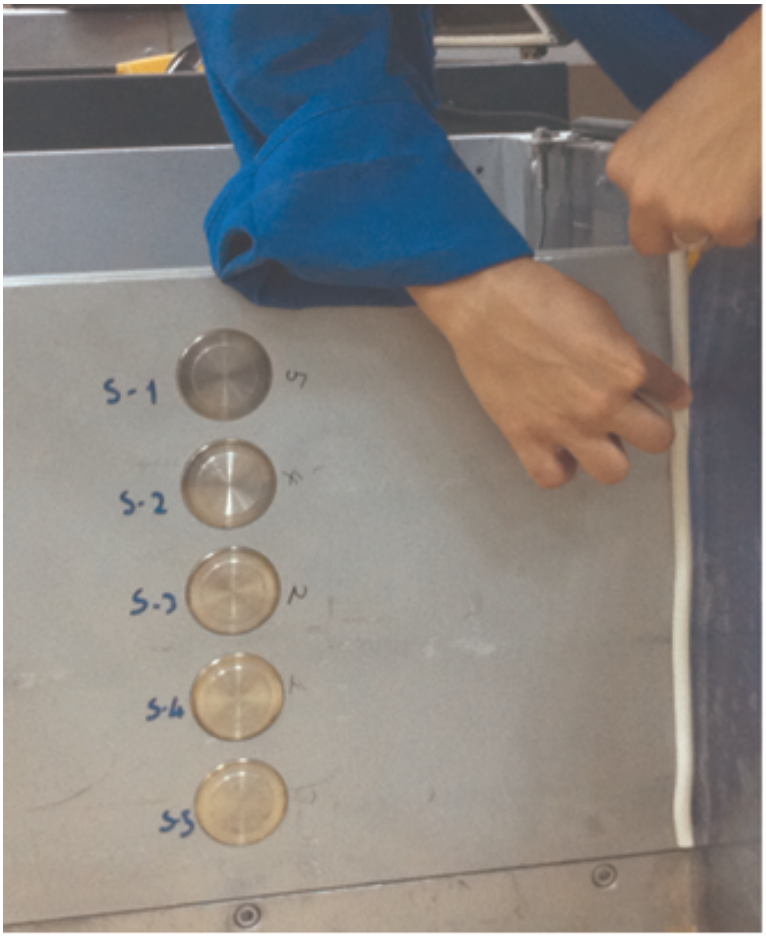

Figure 4.8. The implementation of the sticking material on the edges.

4.1.1.5. Particle image velocimetry (PIV) Analysis. PIV analysis will be used as the deformation measurement system. This technique was developed by (Adrian, 1991) for the field of experimental fluid mechanics. After his studies, the technique was implemented in geotechnical testing. PIV operates by tracking the texture within an image of soil through a series of images. For obtaining the data used in this technique, the tests are recorded through the transparent plexiglass side walls. These walls are covered by transparent film to avoid scratching. In addition to the PIV technique, for the purposes of direct visual interpretation of deformations, a grid of observation patches will be drawn.

4.2. Problems and Solutions

After finishing the construction of the model setup, several control experiments were conducted. The aim of these control experiments was to assess and pinpoint possible design, software and manufacturing problems that might reduce the quality of the tests or that might altogether prevent us from conducting the tests. Several problems were identified which are listed below:

(i) Sensors which are located on the retaining wall were not measuring the values less than 2 kPa. Therefore, correct values were not obtained for the active and at-rest conditions. In addition to this, passive earth pressure test results were inaccurate. The reason of the problems were investigated and concluded that the circuit board were inadequate to convert the analog data to digital. Moreover, the noise coming from the electric circuit was not filtered, leading to the fluctuation of the obtained results. To solve the problem and to obtain definite and accurate results, the initial circuit board system has been replaced with LabVIEW software and its data acquisition system.

(ii) The sides of the testing tank were made by plexiglass and steel profiles. During the tests, which were done to obtain the passive earth pressure coefficient, these sides were deflected due to inadequate steel profiles. To solve the problem, extra profiles were added to reinforce these sides.

(iii) In order to obtain desired relative density, dry-pluvation method was used. During the pluviation, some mechanical problems were observed. The system, which is used for pluviation, has a manually controlled long gap through which the sand pluviates. However, it was not possible to maintain a uniform opening along the manually opened gap. Moreover, it was not possible to quickly open and close the gap to the desired size which decreases the uniformity of the backfill soil. Hence, a new pluviation set-up is designed that uses a funnel and a pipe to pour the sand. The pluviation set-up is carried using the mobile crane. This way it is easier to prepare the models uniformly at the predetermined relative density.

(iv) The mobile crane was used to transfer the sand from storage tank to testing tank and vice versa. However, the height of the crane was not enough to lift the cone

and to move it easily. Therefore, the height of the mobile crane was extended with using extra steel profiles. Additionally, the crane height is now adjustable, rendering it more practical for use in other testing programs.

(v) The fourth sensor was malfunctioning. After several tests, finally it was decided to change the sensor since it was understood that the problem was not caused by mechanical or calibration problems. After changing the sensor, the problem was solved.

4.3. Direct Shear Test For The Interface Friction Angle

In order to observe the influence of interface friction angle between the sand-the moving aluminum plate and also the sand-the transparent plexiglass, direct shear box tests were conducted. The results are shown in Figure 4.9 and Figure 4.10 . As a result of these tests, the friction angle for the interface between the sand and the aluminum plate is calculated as 19^o and for the interface between the plexiglass and the sand as 17^o .

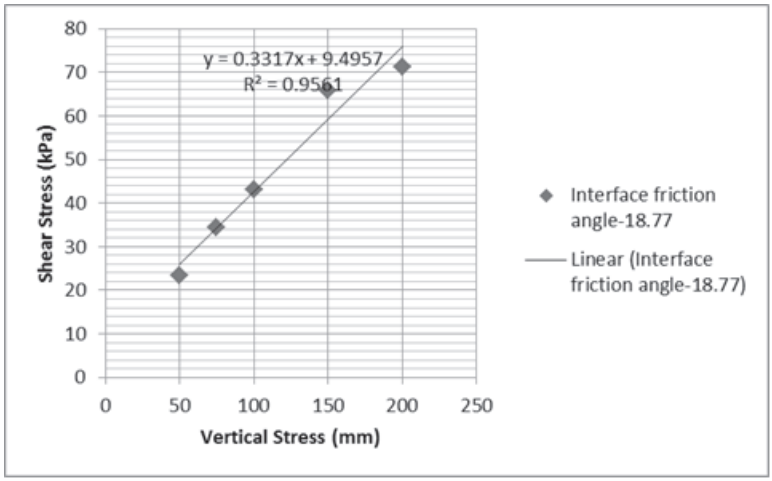

Figure 4.9. Direct shear test result for the determination of interface friction angle between the sand and the moving aluminum plate.

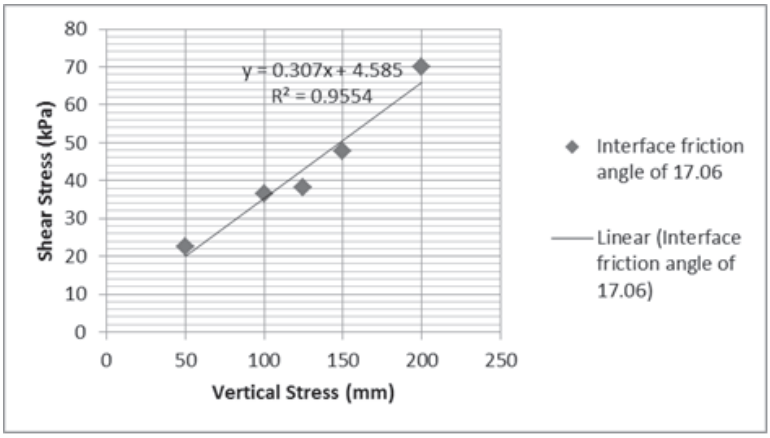

Figure 4.10. Direct shear test line for the interface friction angle between the sand and the plexiglass.

According to Coulomb Method, the friction between the wall and soil ranges from $\phi/2$ to $2\phi/3$, so the results are reasonable.

5. EXPERIMENTAL RESULTS AND DISCUSSION

This sections reports the results of the preliminary tests conducted using the retaining wall model. In these tests, the variation of lateral earth pressure with the horizontal translation of the wall was investigated. Additionally, the coefficient of lateral earth pressure for at rest condition was investigated.

5.1. Test Setup

Four tests were conducted at the same relative density in order to make sure that the small scale retaining wall model is working with the desired quality. Two of these tests were run up to active failure and the others were run up to passive failure. The unit weight of the backfill was measured using three density cans. The sand was pluviated from a height of 28 cm using a funnel and pipe set-up as explaned in the previous sections. The pluviation height was chosen in order to prepare the sample in a loose state. The average unit weight of the sand was calculated using the measurements from the density cans. The relative density of the backfill soil is calculated using the average unit weight. Table 5.1 provides the properties of the backfill soil.

Table 5.1. Summary of testing program.

Sand condition	Relative density, Dr(%)	Unit weight, γ (kN/m^3)	Internal friction angles, ϕ (degrees)	Angle of wall friction between wall-sand , δ (degrees)	Angle of wall friction between wall-plexiglass, δ (degrees)
Loose	32	15	32	19	17

Two pressure transducers were buried in the sand at two different depths to measure the vertical effective stresses within the backfill. The positions of these pressure transducers are 295 mm from the surface (the depth of the 5. transducer) and 110 mm from the surface (the depth of the 2. transducers). The vertical stress at any depth can be calculated simply by using the equation below,

$$\sigma' = \gamma_d . Z \tag{5.1}$$

The vertical effective stresses measured by the two backfill transducers are shown in Figure. The measurements (Figure 5.1) are compared with the vertical effective stresses calculated using the measured vertical effective stresses (Table 5.2). It can be observed that the calculated measurements are in good agreement the calculations using the unit weights.

Table 5.2. The calculation of vertical effective stress to prove unit weights.

Unit weight (kN/m3)	15	15
Depth (mm)	0.295	0.11
Vertical effective stress (ϕ')	4425	1.65

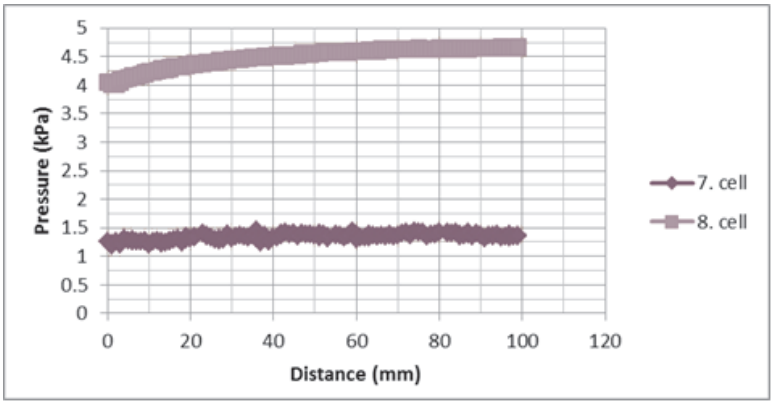

Figure 5.1. Vertical effective stress obtained from the passive pressure test.

5.2. At Rest State

For conducting the test, the loose backfill had been placed into the testing tank by using dry-pluviation method. When the sand was pouring, the density cans were placed in a staggered scheme in the vertical direction with 9 cm intervals starting from the retaining wall level. Two pressure sensors were located towards the end of testing tank within the sand mass in order to measure vertical effective stress.

5.2.1. The test results during the at rest state

The variations of the lateral earth pressure with depth for all tests are shown in Figure 5.2. The distribution of the lateral pressure can be considered to be approxi-

mately linear. Small fluctuations can be attributed to voltage changes.

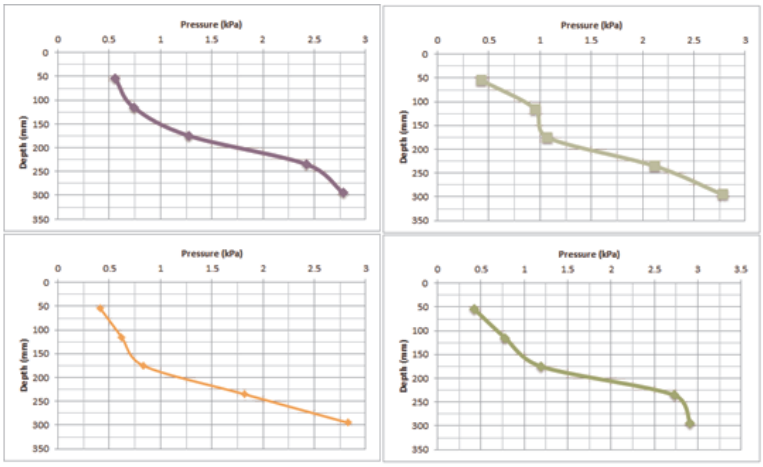

Figure 5.2. Variation of lateral earth pressure with depth.

Figure 5.3 shows all the at-rest pressure-depth relationships on a single figure for comparison.

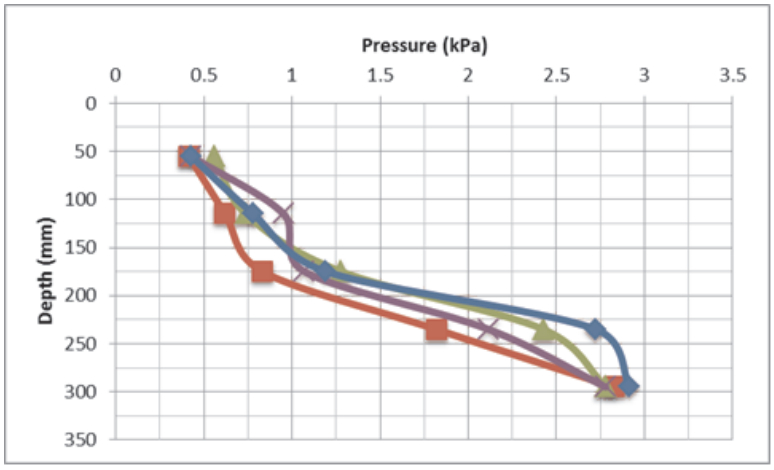

Figure 5.3. Variation of lateral earth pressure with depth.

The results of K_o using a small scale retaining wall were presented and compared with Jaky's formula as shown in Figure 5.4. K_o values obtained from the average of four experiments are compared with Jaky's formula. The first, second and third sensors are in good agreement with his formula whereas the fourth and fifth are in fairly good agreement.

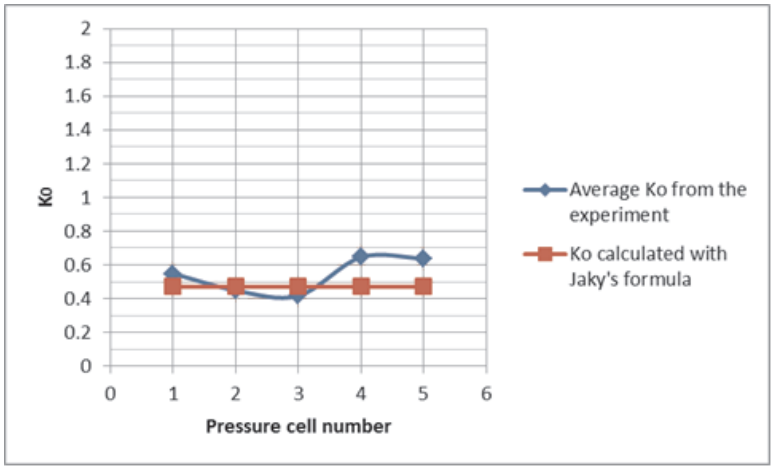

Figure 5.4. Results of K_o values which were obtained experiments and Jaky's formula.

Hanna and Al-Romhein (2008), Michalowski (2005) asserted that the theoretical values calculated by the Jacky's formula are a good representation for normally consolidated loose samples at rest. However, Wanatowski and Chu (2007) claimed that K_o values obtained from the both triaxial tests and plane strain tests does not agree with Jaky's equation. Additionally, Guo (2009) suggested that the coefficient of earth pressure at rest K_o of granular materials is not a unique function of neither the critical friction angle, ϕ_{cv}, nor the peak friction angle, ϕ_{peak} He illustrated that the effect of density and stress level on K_o should be considered.

Based on the results of the conducted experiments and the literature survey, it can be said that small scale retaining wall mode can be used to calculate K_o values. The experiments for measuring K_o values for normally consolidated loose sand were successful.

The results show that the K_o values for normally consolidated loose sand can be calculated using Jacky's formula as Hanna and Al-Romhein (2008) and Michalowski (2005) proposed.

5.3. Investigation of the Lateral Earth Pressures During Passive Mode of Deformation

During the passive mode of deformation tests, the retaining wall slowly moved towards the soil mass in translational mode at a constant speed of 3 mm/s. The wall movements were adjusted using the program that controls the movements of the wall back and forth. The LABVIEW system was switched to record the readings and the wall started to move toward the sand mass. The passive pressure increased and eventually a limiting passive pressure was reached. During the retaining wall translation, the camera recorded the tests through the plexiglass sidewalls for later investigation.

5.3.1. The Results of the Passive Type of deformation tests

The variation of passive earth pressure measured by pressure transducers is shown in Figure 5.5. As can be seen, the data coming from the device corresponds to a type of behavior that is expected from a loose specimen. In order to make sure that the model is operating properly, the results of the two experiments, which have same properties, are compared in the same graphs as shown in Figure 5.7. These results are approximately the same; therefore the device measurements are consistent, and therefore the tests are repeatable.

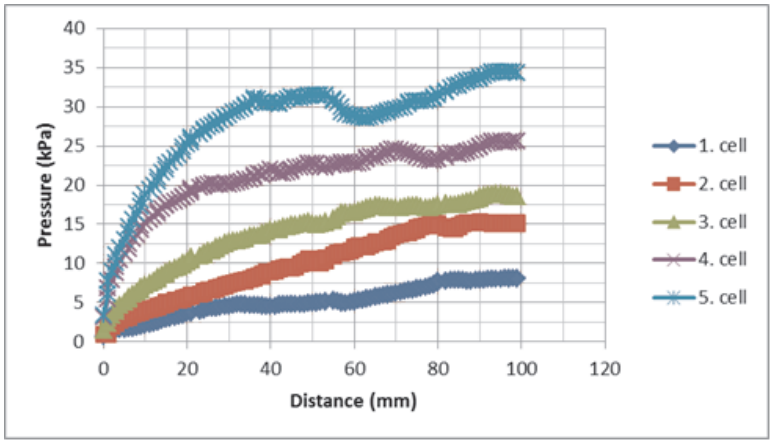

Figure 5.5. Variation of passive earth pressure with displacement at test-1.

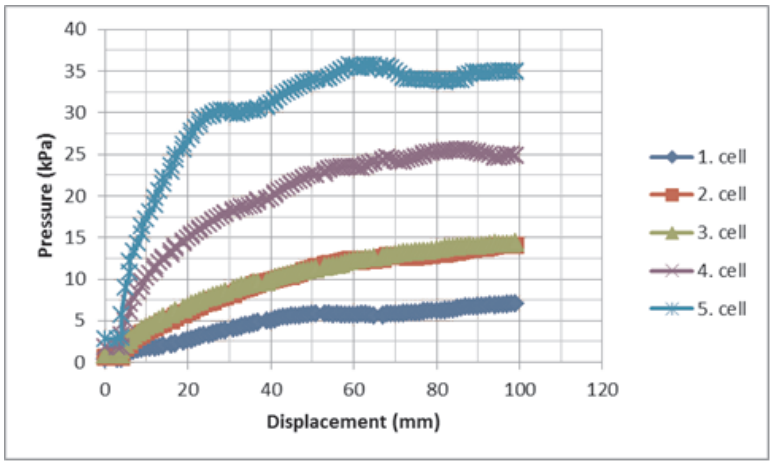

Figure 5.6. Variation of passive earth pressure with displacement at test-2.

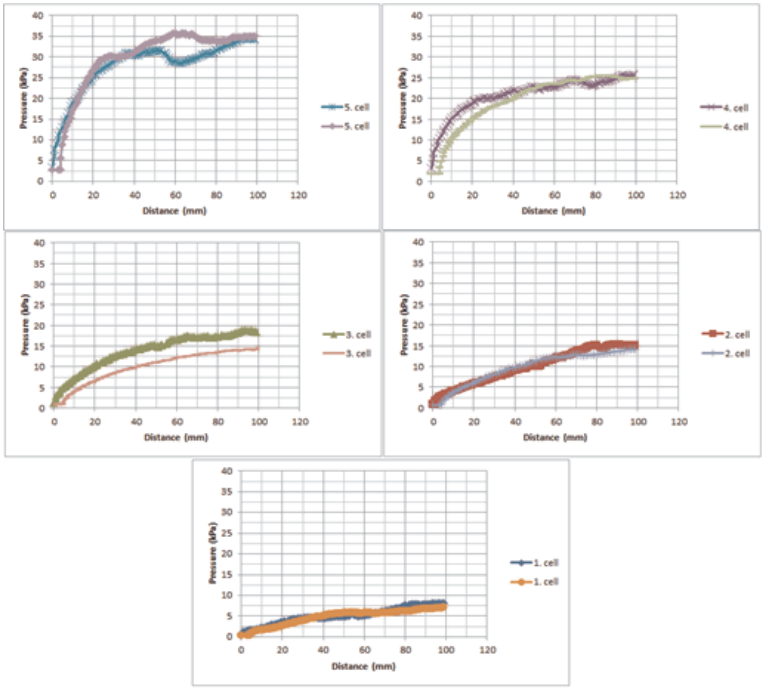

Figure 5.7. Variation of passive earth pressure with displacement at each transducers.

The variation of horizontal earth-pressure coefficient K_p as a function of wall displacement is shown in Figure 5.8. It can be seen that Coulomb theory is in good agreement with the passive thrust against the retaining wall with a normally consolidated loose backfill. However, Rankine theory underestimates the passive earth pressure. It can be attributed to the fact that Rankine theory does not to take into accounts the friction effect between the wall surface and backfill.

According to Narain and Nandakkumaran (1969), the maximum passive earth pressure obtained at a wall displacement accounting to 8.6% when translating in loose backfill. Fang *et al.* (1994, 2001) claimed that as the wall movement exceeded 12% of the wall height, the passive earth pressure would reach the maximum constant value, regardless of the initial density. The presented soils approximately reached the constant values when the wall movement reached 9.6% of the wall height.

Passive earth pressure coefficient increased with wall movements until a maximum value was reached (Narain and Nandakkumaran, 1969). Similar results were obtained by Rowe and Peaker (1965), and Fang *et al.* (2001). Fang *et al.* (1994, 2001) indicated that Rankine theory underestimated the passive thrust, whereas Coulomb theory provides a slightly underestimated passive thrust for the loose backfill. However, he also indicated that Coulomb theory overestimated the passive trust for the dense backfill. Fang *et al.* (1994, 2001) recommended that the dilation and the strength reduction of the dense backfill should be considered.

Figure 5.8 shows the variation of coefficient K_p as a function of wall movement. The distribution of the lateral earth pressure coefficient measured with pressure sensors are individually calculated at different depths where the transducers located. As can be seen, the passive earth pressure coefficient increased with wall movements until a maximum value. The experiments show that K_p values slightly underestimated the passive thrust with the values calculated with the Coulomb theory except the fifth one. The data from the fifth sensor is in good agreement with the Coulomb theory as shown in Figure 5.9. However, Rankine theory underestimates the passive earth pressure as indicated Fang *et al.* (1994, 2001). Little discrepancies can be found between the results of each transducer. These differences can be attributed to the nonlinear distributions of pressures until the failure point. This inference can be investigated in detail by means of small scale retaining wall model tests.

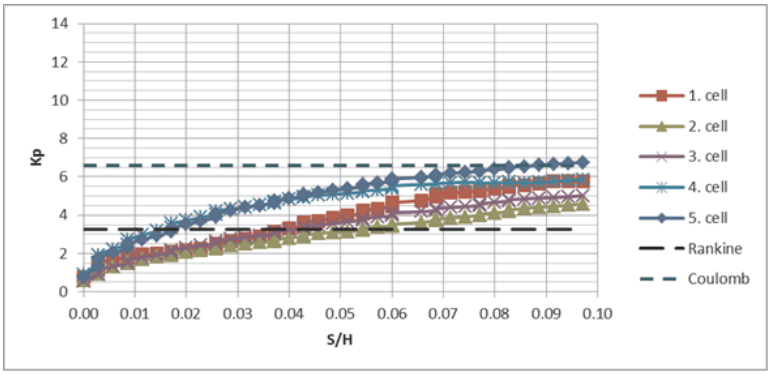

Figure 5.8. Variation of K_p with wall movement for loose sand at all transducers.

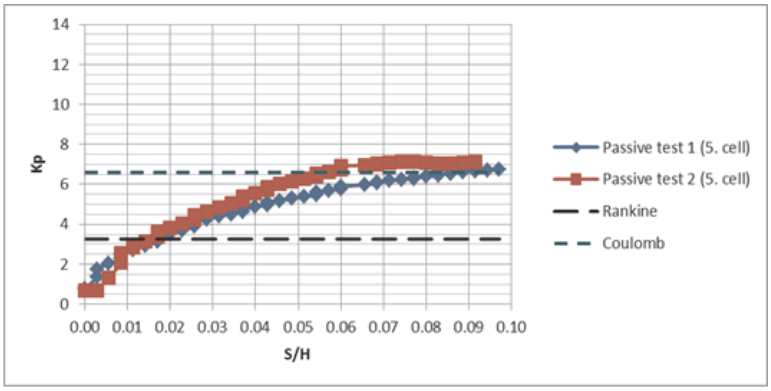

Figure 5.9. Variation of K_p with wall movement for loose sand at the fifth transducer.

The load-displacement curve directly measured from the load cell readings is shown in Figure 5.10. As can be seen, the loads increased with wall movements.

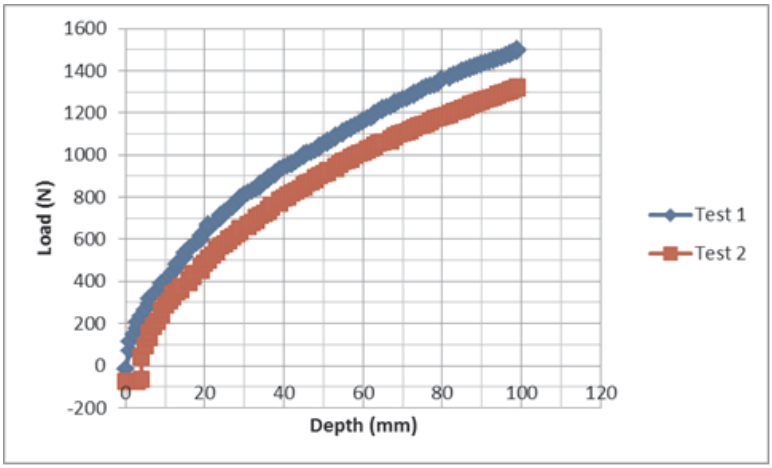

Figure 5.10. Typical load-displacement curve for loose normally consolidated sand.

Narain and Nandakkumaran (1969) claimed that pressure distribution along the wall height was linear for the translational wall movement. The pressure distribution along the pressure transducers are illustrated in Figure 5.11. It can be said that the distributions are approximately linear at failure point as Narain and Nandakkumaran (1969) indicated.

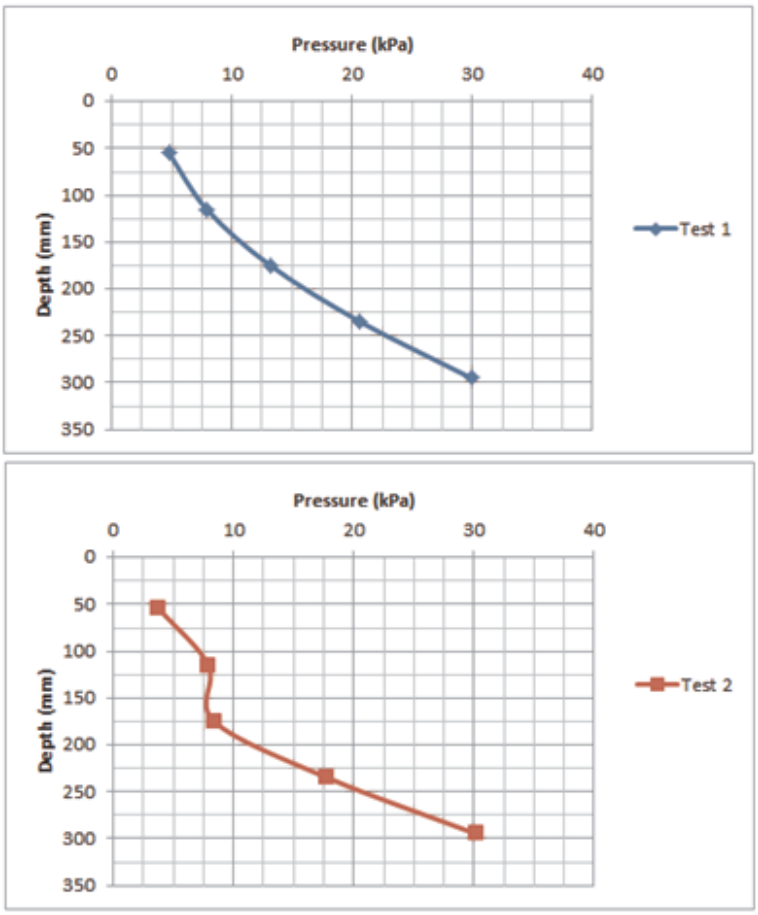

Figure 5.11. The variation of passive earth pressure with depth at selected point.

5.4. Investigation of the Lateral Earth Pressures During Active Mode of Deformation

During the active mode of deformation tests, the retaining wall was slowly moved away from the soil mass in translational mode at a constant speed of 3 mm/s. The wall movements were adjusted using the program that controls the movements of the wall back and forth. The LabVIEW system was switched to record the readings and the wall started to move away from the sand mass. The active pressure increased and

eventually a limiting active pressure was reached. When the retaining wall was moving, the camera was recording the tests for later investigation.

5.4.1. The Results of the Active mode of deformation tests

The variations of active earth pressure throughout the tests as measured by pressure transducers are shown in Figure 5.12 and Figure 5.13. As can be seen, the data corresponds to the expected behavior of loose specimen. In order to make sure that the system is working properly, the results of two experiments with similar properties are compared in Figure 5.14. The results are approximately the same; therefore the measurements of the testing system are consistent and reliable.

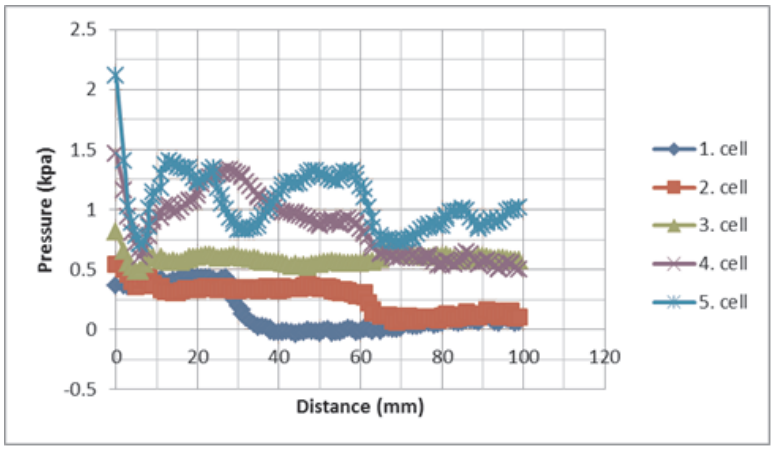

Figure 5.12. Variation of active earth pressure with displacement at test-1.

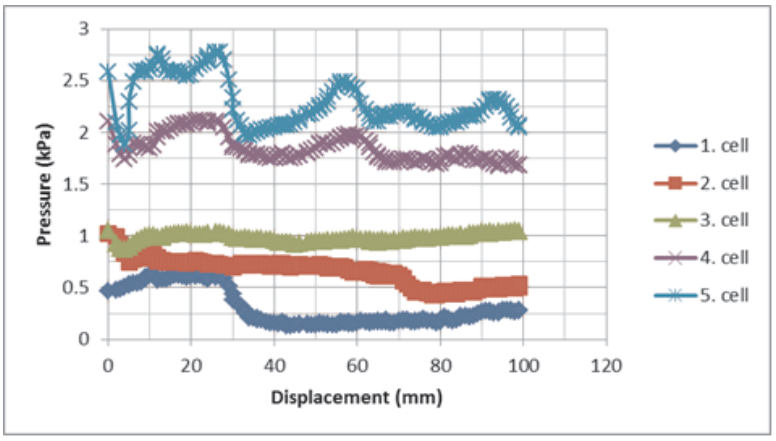

Figure 5.13. Variation of active earth pressure with displacement at test-1.

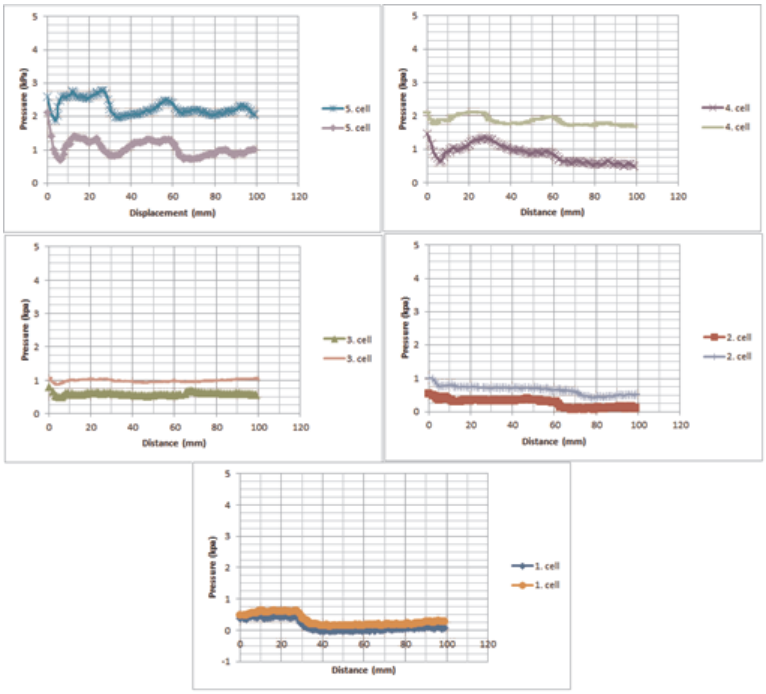

Figure 5.14. Variation of active earth pressure with displacement at each transducer.

Handy (1985), Fang and Ishibashi (1986), Paik and Salgado (2003) and Goel and Patra (2008) claimed that the distribution of active earth pressure behind the wall is non-linear due to the effects of principal stress rotation, arching effects and mode of wall movement. Goel and Patra (2008) suggested that the ratio of the height of the point of application of the lateral active force to the wall height is independent of wall height for all formulations.

Figure 5.15 shows the variation of coefficient K_a as a function of wall movement. The distributions of the lateral earth pressure coefficient measured with pressure sensors are individually calculated at different depths where the transducers located. As can be seen, the active earth pressure coefficient decreased with wall movements until a maximum value. The experiments show that K_a values obtained from the fifth and fourth sensors overestimated the passive thrust calculated using Coulomb and Rankine theory at the beginning of the test, but at the failure point they are in good agreement with the theories. However, K_p values obtained from the third and second sensors are in fairly good agreement with these theories. The first sensor behavior could not reflect the behavior due to having a very small amount of sand on it. To be more precise,

when the wall started to move away from the backfill, the surface level of the sand dropped in height, exposing the first sensor. As a result, the result of the first sensor is excluded from the discussion.

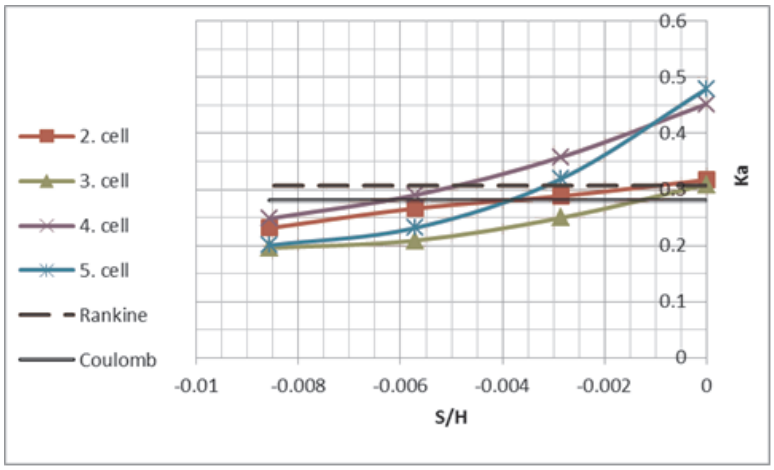

Figure 5.15. Variation of K_p with wall movement for loose sand at all transducers.

The pressure distribution along the height of the retaining wall is illustrated in Figure 5.16. It can be claimed that the distributions are non-linear at failure point as Handy (1985), Fang and Ishibashi (1986), Paik and Salgado (2003) and Goel and Patra (2008) indicated.

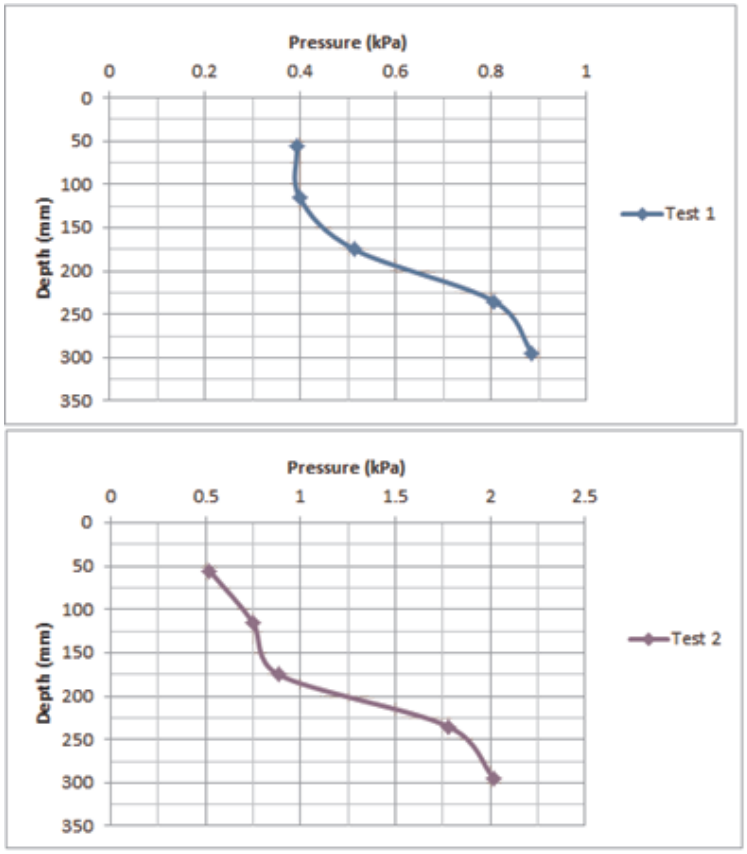

Figure 5.16. The variation of passive earth pressure with depth at selected point.

The load-displacement curve directly measured from the load cell readings is shown in Figure 5.17. As can be seen, the loads decreased with wall movements.

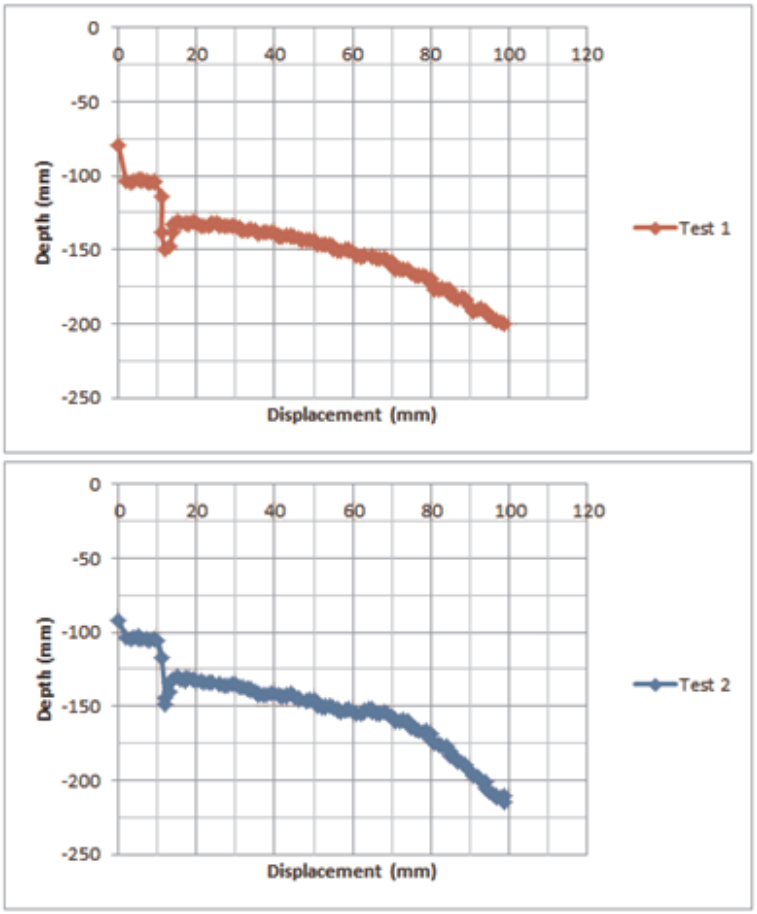

Figure 5.17. Typical load-displacement curve for loose normally consolidated sand.

5.5. K_o-K_a and K_o-K_p Relationships

K_o-K_a and K_o-K_p relationships were defined using the fifth sensor data as shown in Figure. As can be seen, the coefficient K_p increased with increasing wall movement until a maximum value was reached, then remained approximately constant and also K_a decreased until a minimum value was reached and then remained constant. The passive state is more resistant to failure. Therefore it may be possible to claim that geotechnical structures are more prone to fail with an active mode of deformation.

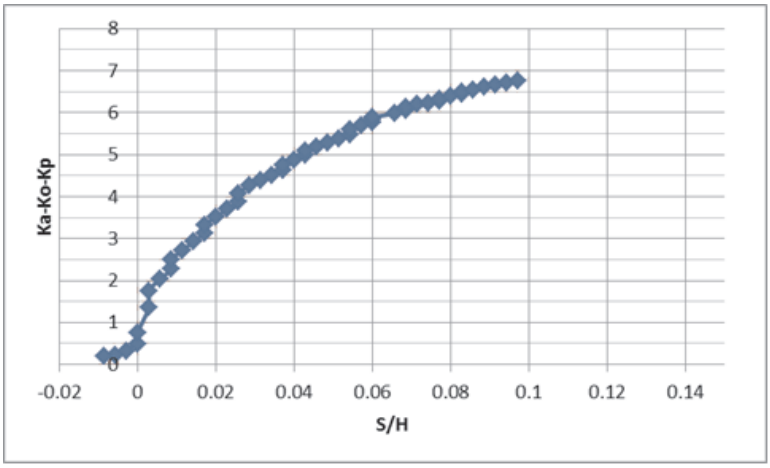

Figure 5.18. K_o-K_a and K_o-K_p Relationships.

6. CONCLUSION

In this study, a new small scale retaning wall model was designed to investigate the lateral earth pressure coefficients of cohesionless soils. This model consists of a testing tank, a retaining wall, a sand pluviation system, a storage tank, a mobile crane and software. The model is designed to impose a plane strain model of deformation on the backfill soil. Dry-pluviation method is used in the experiment to achieved desired relative density. Unit weights of the backfill are measured by means of density cans. LabVIEW system design software is used as an analog to digital converter and as a software interface. Some problems occurred while designing and setting up the model. These problems are defined and the solutions are explained in this thesis.

Constructed physical model provides the opportunity for investigating the variation of lateral earth pressure with deformation. Additionally, it allows the definition of K_o-K_a and K_o-K_p relationships based on different relative densities and overconsolidation ratio combinations. This way, it will be possible to correctly estimate the magnitude and distribution of the lateral earth pressures acting on geotechnical structures.

Several trial tests were conducted to confirm the working quality of the model setup. The results were compared with the theories and previous research in the field. It is observed that the model works accurately, and the tests are repeatable. Test results were evaluated and some interpretations were made, and it is shown that the small scale retaining wall model system is functioning properly and yielding reliable data for future use in the investigation of the lateral earth pressure coefficients of cohesionless backfill soils.

REFERENCES

Adrian, R.J., 1991, "Particle Imaging Techniques for Experimental Fluid Mechanics". *Annual Review of Fluid Mechanics*. Vol. 23, pp. 261-304.

American Society for Testing and Materials, 2006, "American Society for Testing and Materials, Standard Test Methods for Specific Gravity of Soil Solids by Water Pycnometer", *ASTM Standards: D854*.

American Society for Testing and Materials, 2007, "Standard Test Method for Particle-Size Analysis of Soils", *ASTM Standards: D422-63*.

American Society for Testing and Materials, 2009, "Standard Specification for Woven Wire Test Sieve Cloth and Test Sieves", *ASTM Standards: E11*.

American Society for Testing and Materials, 2006, "Standard Test Methods for Minimum Index Density and Unit Weight of Soils and Calculation of Relative Density", *ASTM Standarts: D4254*.

American Society for Testing and Materials, 2006, "Standard Test Methods for Maximum Index Density and Unit weight of Soils Using a Vibratory Table" , *ASTM Standarts: D4253*.

Bardet, J.P., 1997, *Experimental Soil Mechanics*, *Prentice Hall*, New Jersey.

Bishop, A.W., 1966, "The Strength of soil as Engineering Materials", *Sixth Rankine lecture, Géotechnique*, Vol. 16, No. 2, pp. 91-130.

Bolton, M.D., 1986, "The Strength and Dilatancy of Sands", *Géotechnique*, Vol. 36, No.1, pp. 65-78.

Coulomb, C.A., 1776, "Essai Sur Une Application Des Regles de Maximis et Minimis à Quelques Problèmes de Statique", *Relatifs à l'Architecture, Memoires de l'Academie Royale Pres Divers Savants*, Vol.3, pp. 343-382,

Caquot, A., and L. Kerisel, 1948, *Tables de Poussee et Butee*, *Gauthier-Villars*, Paris.

D'Appolonia, D.J., R.V., Whitman, and E., D'Appolonia, 1969, "Sand Compaction with Vibratory Rollers", *Journal of Soil Mechanics and Foundation Engineering Division*, Vol. 95, No. SM1, pp. 263-284.

Das, B.M., 1990, *Principles of Foundation Engineering*, 2nd Ed., *PWSKent*, Boston.

Brinch-Hansen, J., 1953, *Earth Pressure Calculation, Danish Technical Press*, *Copenhagen*, Denmark.

Duncan, J.M. and R.L., Mokwa, 2001, "Passive Earth Pressures: Theory and Tests", *Journal of Geotechnical and Geoenvironmental Engineering, ASCE*, Vol.127, No. 3, pp. 248-57.

Duncan, J.M., and R.B., Seed, 1986, "Compaction-Induced Earth Pressures Under Ko Conditions", *Journal of Geotechnical. Engineering*, Vol.112, No. 1, pp. 1-22.

Fang, Y.S. and I., Ishibashi, 1986, "Static Earth Pressures with Various Wall Movements", *Journal of Geotechnical Engineering, ASCE*, Vol.112, No. 3, pp. 317-33.

Fang, Y.S., T.J., Chen and B.F., Wu, 1994, "Passive Earth Pressures with Various Wall Movements", *Journal of Geotechnical Engineering, ASCE*, Vol.120, pp. 1307-23.

Fang, Y.S., C.C., Lee and T.J., Chen, 2006, "Passive Earth Pressure with Various Backfill Densities", *Physical Modelling in Geotechnics-6th* ICMPG'6-Ng, London, England.

Feda, J. 1984, "K_o-Coefficient of Sand in Triaxial Apparatus", *Journal of Geotechnical Engineering*, Vol.110, No.4, pp. 519-524.

Goel, S. and N.R., Patra, 2008, "Effect of Arching on Active Earth Pressure for Rigid Retaining Walls Considering Translation Mode", *International Journal of Geomechanics, ASCE*, Vol.8, No. 2, pp. 123-133.

Guo, P., 2010, "Effect of Density and Compressibility on K_0 of Cohesionless Soils", *Acta Geotechnica*, Vol. 5, No. 4, pp. 225-238.

Handy, R.L., 1985, "The arch in soil arching", *Journal of Geotechnical. Engineering, ASCE*, Vol.111, No. 3, pp. 302-318.

Hanna, A.M., and A.M. Ghaly, 1992, "Effects of Ko and Overconsolidation on Uplift Capacity", *Journal of Geotechnical. Engineering*, Vol.118, pp. 1449-1469.

Hanna, A. and I., Al-Khoury, "Passive Earth Pressure of Overconsolidated Cohesionless Backfill", *Journal of Geotechnical and Geoenvironmental Engineering, ASCE*, Vol.131, No. 8, pp. 978-86.

Hanna, A. and I., Romhein, 2008, "At Rest Earth Pressure of Overconsolidated Cohesionless Backfill", *Journal of Geotechnical and Geoenvironmental Engineering*, Vol. 134, No. 3, pp. 408-412.

Harrop-Williams, K.O., 1989, "Geostatic wall Pressures", *Journal of Geotechnical. Engineering, ASCE* 115, No. 9, pp. 1321-1325.

Holtz, R.D. and W.D., Kovacs, 1981, *An Introduction to Geotechnical Engineering*, *Prentice-Hall, Englewood Cliffs*, N.J.

Jaky, J., 1944, "The Coefficient of Earth Pressure At-rest", *J. Society of Hungarian Architects and Engineers*, pp. 355-358.

Janssen, H.A., 1985, "Versuche über Getreidedruck in Silozellen", *Zeitschr d Vereines Deutscher Ingenieure*, Vol. 39, No. 35, pp. 1045-1049.

Janbu, N., 1957, "Earth Pressure and Bearing Capacity Calculations by Generalized

Procedure of Slices", *Proceedings., 4th Int. Conf. on Soil Mechanics and Foundations Engineering*, London, No. 2, pp. 207-212.

Lee, K.L., 1970, "Comparison of Plane Strain and Triaxial Tests on Sand", *J. Soil Mech. Found. Div.*, Vol. 96, No. 3, pp. 901-923.

Mayne, P. and F.H., Kulhawy, 1982, "Ko OCR Relationships in Soils", *Journal of Geotechnical. Engineering*, Vol.108, No. 6, pp. 851-872.

Marachi, N., J., Duncan, C., Chan, and H.S, eed, 1981, "Plane-Strain Testing of Sand", *Laboratory Shear Strength of Soils, ASTM STP 740*, R. N. Yong, and F. C. Townsend, eds., ASTM, pp. 294-302.

Mesri, G., and T.M., Hayat, 1993, "The Coefficient of Earth Pressure At-rest", *Canadian Geotechnical Journal*, Vol.30, No. 4, pp. 647-666.

Meyerhof, G.G., 1976, "Bearing Capacity and Settlement of Pile Foundations", *Journal of Geotechnical. Engineering*, Vol.102, No.3, pp. 195-228.

Michalowski, R.L., 2005, "Coefficient of Earth Pressure At-rest", *Journal of Geotechnical and Geoenvironmental Engineering*, Vol. 131, No. 11, pp. 1429-1433.

Narain, J., S., Saran and P., Nandakumaran, 1969, "Model Study of Passive Pressure in Sand", *Journal of Soil Mechanics and Foundation Engineering Division, ASCE*, Vol.95, pp. 969-83.

Okochi, Y. and F., Tatsuoka, 1984, "Some Factors Affecting Ko Values of Sand Measured in Triaxial Cell", *Soils and Foundations, Japan Society of Soil Mechanics and Foundation Engineering*, Vol. 24, No. 3, pp. 52-68.

Paik, K.H. and R., Salgado, 2003, "Estimation of Active Earth Pressure Against Rigid Retaining Walls Considering Arching Effects", *Geotechnique*, Vol.53, No. 7, pp. 643-53.

Rankine, W.M.J., 1857, "On Stability on Loose Earth", *Philisophic Transactions of Royal Society*, London, Part I, pp. 9-27.

Rowe, P.W. and K., Peaker, 1965, "Passive Earth Pressure Measurements", *Geotechnique*, Vol.15, pp. 57-78.

Rowe, P.W., 1969, "The Relationship Between the Shear Strength of Sands in Triaxial Compression", *Plane Strain and Direct Shear, Géotechnique*, Vol. 19, No.1, pp.75-86.

Sokolovski, V.V., 1960, *Statics of Soil Media*, *Butterworths*, London.

Terzaghi, K., 1920, "Old Earth Pressure Theories and New Test Results" *English News-Recordings*, Vol. 85, No. 14, pp. 14-32.

Terzaghi, K., 1932, "Record Earth Pressure Testing Machine", *Engineering News Record*, No. 109, pp. 365-9.

Terzaghi, K., 1934, "Large Retaining Wall Tests", *Engineering News Record*.

Terzaghi, K., 1936, "A Fundamental Fallacy in Earth Pressure Computations", *Journal of the Bostan Society of Civil Engineers*, Vol. 23, No. 2, pp. 71-88.

Terzaghi, K., 1941, "General Wedge Theory of Earth Pressure", *ASCE Transactions*, Vol. 106, No. 2099, pp. 68-80.

Terzaghi, K., 1943, *Theoretical Soil Mechanics*, *Wiley*, New York.

Terzaghi, K. and R.B., Peck, 1967, *Soil Mechanics in Engineering Practice*, *2nd Ed., Wiley*, New York.

Terzaghi, K., R.B., Peck, and G., Mezri, 1996, *Soil Mechanics in Engineering Practice*, *3rd Ed., Wiley*, New York.

Tejchman, J., E., Bauer and S.F., Tantono, 2007, "Influence of Initial Density of Cohesionless Soil on Evolution of Passive Earth Pressure", *Acta Geotechnica*, Vol. 2, No. 1, pp.53-63.

Tsagareli, Z.V., 1965, "Experimental Investigation of the Pressure of a Loose Medium on Retaining Walls with a Vertical Back Face and Horizontal Backfill Surface", *Journal of Soil Mechanics and Foundation Engineering Division*, Vol. 91, No. 4, pp. 197-200.

Wanatowski, D. and J., Chu, 2007, "Ko of Sand Measured by a Plane-Starin Apparatus", *Canadian Geotechnical Journal*, Vol.44, pp. 1006-1012.

Wroth, C.P., 1973, "General Theories of Earth Pressure and Deformation", *Proceedings, 5th European Conference on Soil Mechanics and Foundation Engineering*, Madrid, Spain.

White, D.J., W.A., Take and M.D., Bolton, 2003, "Ge´otechnique" Vol. 53, No. 7, pp. 619-631.

Vardoulakis, I.G., 1977, "Scherfugenbildung in Sandkörpern als Verzweigungsproblem", Ph.D. Thesis, *Institutes für Bodenmechanik und Felsmechanik der Universität Fridericiana in Karlsruhe.*

Vermeer, P.A., 1990, "The Orientation of Shear Bands in Biaxial Tests", *Géotechnique* Vol. 40, No. 2, p. 223-236.